Mid-Holocene Climate Change over China: Model-Data Discrepancy

Yating Lin [1,2,4], Gilles Ramstein [2], Haibin Wu [1,3,4], Raj Rani [2], Pascale Braconnot [2], Masa Kageyama [2], Qin Li [1,3], Yunli Luo [5], Ran Zhang [6] and Zhengtang Guo [1,3,4]

1. Key Laboratory of Cenozoic Geology and Environment, Institute of Geology and Geophysics, Chinese Academy of Sciences, Beijing 100029, China

2. Laboratoire des Sciences du Climat et de l'Environnement, LSCE/IPSL, CEA-CNRS-UVSQ, Université Paris-Saclay, Gif-sur-Yvette 91191, France

3. CAS Center for Excellence in Life and Paleoenvironment, Beijing, 100044, China

4. University of Chinese Academy of Sciences, Beijing 100049, China

5. Institute of Botany, Chinese Academy of Sciences, Beijing 100093, China

6. Institute of Atmospheric Physics, Chinese Academy of Sciences, Beijing 100029, China

Abstract:

The mid-Holocene period (MH) has long been an ideal target for the validation of Global Circulation Model (GCM) results against reconstructions gathered in global datasets. These studies aim to test the GCM sensitivity mainly to the seasonal changes induced by the orbital parameters (longitude of the perihelion). Despite widespread agreement between model results and data on the MH climate, some important differences still exist. There is no consensus on the continental size (the area of the temperature anomaly) of the MH thermal climate response, which makes regional quantitative reconstruction critical to obtain a comprehensive understanding of the MH climate patterns. Here, we compare the annual and seasonal outputs from the most recent Paleoclimate Modelling Intercomparison Project Phase 3 (PMIP3) models with an updated synthesis of climate reconstruction over China, including, for the first time, a seasonal cycle of temperature and precipitation. Our results indicate that the main discrepancies between model and data for the MH climate are the annual and winter mean temperature. A warmer-than-present climate condition is derived from pollen data for both annual mean

temperature (~0.7 K on average) and winter mean temperature (~1 K on average), while most of the models provide both colder-than-present annual and winter mean temperature and a relatively warmer summer, showing linear response driven by the seasonal forcing. By conducting simulations in BIOME4 and CESM, we show that the surface processes are the key factors drawing the uncertainties between models and data. These results pinpoint the crucial importance of including the non-linear responses of the surface water and energy balance to vegetation changes.

Keywords: PMIP3 Pollen data Inverse Vegetation Model Seasonal climate change

1. Introduction

Much attention of paleoclimate studies has been focused on the current interglacial (the Holocene), especially the mid-Holocene (MH, 6±0.5 ka). The major difference in the experimental configuration between the MH and pre-Industrial (PI) arises from the orbital parameters which brings about an increase in the amplitude of the seasonal cycle of insolation of the Northern Hemisphere and a decrease in the Southern Hemisphere (Berger, 1978). Thus, the MH provides an excellent case study on which to base an evaluation of the climate response to changes in the distribution of insolation. Great efforts have been devoted by the modeling community to design of MH common experiments using similar boundary conditions (Joussaume and Taylor., 1995; Harrison et al., 2002; Braconnot et al., 2007a, b). In addition, much work has been done to reconstruct the paleoclimate change based on different proxies at global and continental scale (Guiot et al., 1993; Kohfeld and Harrison, 2000; Prentice et al.,

2000; Bartlein et al., 2011). The greatest progress in understanding the MH climate change and variability has consistently been made by comparing large-scale analyses of data with simulations from global climate models (Joussaume et al., 1999; Liu et al., 2004; Harrison et al., 2014).

However, the source of discrepancies between model results and data is still an open and stimulating question. Two types of inconsistencies have been identified: 1) where the model and data show opposite signs, for instance, paleoclimate evidence from data-records indicates an increase of about 0.5 K in global annual mean temperature during the MH compared with PI (Shakun et al.. 2012; Marcott et al., 2013), while there is a cooling trend in model simulations (Liu et al., 2014). 2) where the same trend is displayed by both model and data but with different magnitudes. Previous studies have shown that while climate models can successfully reproduce the direction and large-scale patterns of past climate changes, they tend to consistently underestimate the magnitude of change in the monsoons of the Northern Hemisphere as well as the amount of the MH precipitation over northern Africa (Braconnot et al., 2012; Harrison et al., 2015). Moreover, significant spatial variability has been noted in both observations and simulations (Peyron et al., 2000; Davis et al., 2003; Braconnot et al., 2007a; Wu et al., 2007; Bartlein et al., 2011). For instance, Marcott et al. (2013) reconstructed a cooling trend of global temperature during Holocene, mainly from the marine records (~80%). While based on 642 sub-fossil pollen data, Marsicek et al. (2018) shows a long-term warming defined the Holocene until around 2000 years ago for Europe and North America continents. The different trends of pollen- and marine-based reconstruction indicate the spatial variability of annual temperature change during MH over the globe, which has already been investigated by Bartlein et al. (2010). That makes regional quantitative reconstruction (Davis et al., 2003; Mauri et al., 2015) essential to obtain a comprehensive understanding of the MH climate patterns, and to act as a benchmark to evaluate climate models (Fischer and Jungclaus, 2011; Harrison et al., 2014;).

China offers two advantages with respect to these issues. The sheer expanse of the country means that the continental response to insolation changes over a large region can be investigated. Moreover, the quantitative reconstruction of seasonal climate changes during the MH, based on the new pollen dataset, provides a unique opportunity to compare the seasonal cycles for models and data. Previous studies indicate that warmer and wetter than present conditions prevailed over China during the MH and that the magnitude of the annual temperature increases varied from 2.4-5.8 K spatially, with an annual precipitation increase in the range of 34-267 mm (e.g., Sun et al., 1996; Jiang et al., 2010; Lu et al., 2012; Chen et al., 2015). However, Jiang et al. (2012) clearly show a mismatch between multi-proxy reconstructions and model simulations. In terms of climate anomalies (MH-PI), besides the ~1 K increase in summer temperature, 35 out of 36 Paleoclimate Modelling Intercomparison Projects (PMIP) models reproduce annual (~0.4 K) and winter temperatures (~1.4 K) that are colder than the baseline, and a drier-than-baseline climate in some western and middle regions over China is depicted in models (Jiang et al., 2013). Jiang et al. (2012) point out the model-data discrepancy over China during the MH, but the lack of seasonal reconstructions in their study limits comparisons with simulations.

An important issue raised by Liu et al. (2014) is that the discrepancy at the annual level could be due to incorrect reconstructions of the seasonal cycle, a key objective in our paper. Moreover, it has been suggested that the vegetation change can strengthen the temperature response in high latitudes (O'Ishi et al., 2009; Otto et al., 2009), as well as alter the hydrological conditions in the tropics (Z. Liu et al., 2007). However, compared to the substantial land cover changes in the MH derived from pollen datasets (Ni et al., 2010; Yu et al., 2000), the changes in vegetation have not yet been fully quantified and discussed in PMIP3 (Taylor et al., 2012).

In this study, we first present new reconstructions. We use a quantitative biomization method to reconstruct vegetation types during the MH, based on a new synthesis of pollen datasets, and then use an Inverse Vegetation Model (Guiot et al., 2000; Wu et al., 2007) to obtain the mean

annual temperature, the mean temperature of the warmest month (MTWA), the mean temperature of the coldest month (MTCO), the mean annual precipitation, July precipitation and January precipitation over China for the MH. Furthermore, we present a comprehensive evaluation of the PMIP3 simulations performed with state-of-art climate models, based on our reconstructions of temperature and precipitation. This is the first time that such a progress towards a quantitative seasonal climate comparison for the MH over China has been made. This point is crucial because the MH PMIP3 experiment is essentially one that looks at the response of the models to changes in the seasonality of insolation, and the attempt to derive reconstructions of both summer and winter climate to compare with the simulations will thus enable us to answer the question posed by Liu et al. (2014) on the importance of seasonal reconstructions.

2. Data and Methodology

2.1 Data

In this study, we collected 159 pollen records, covering most of China, for the MH period (6000±500 ^{14}C yr BP) (Fig. 1). Notably, according to IntCal13 (Reimer et al., 2013), the MH time slice 6000±500 ^{14}C yr BP is about 6800 Cal BP (the average value), which is not totally consistent with the "mid-Holocene" used in CMIP5/PMIP3 experiment (6000 Cal BP). But for a better comparison with BIOME6000 (in which the MH is defined as 6000±500 14C yr BP), we decided to choose the pollen data at 6000±500 14C yr BP in our study. In the 159 records, 65 were from the China Quaternary Pollen Database (CQPD, 2000), three were original datasets obtained for our study, and the others were digitized from pollen diagrams in published papers with a recalculation of pollen percentages based on the total number of terrestrial pollen types. These digitized 91 pollen records were selected according to three criteria: (1) clearly readable pollen diagrams with a reliable chronology with the minimum of three independent age control

123 points since the LGM; (2) including the pollen taxa during 6000±500 ^{14}C yr BP period with a
124 minimum sampling resolution of 1000 years per sample; (3) abandon the pollen records if the
125 published paper mentions the influence of human activity. For the age control, different dating
126 methods are utilized in the collected pollen records, we applied CalPal 2007 (Weninger et al.,
127 2007) to correct ^{14}C age into calendar age so that they can be contrasted with each other. For
128 lacustrine records, if the specific carbon pool age is mentioned in the literature, the calendar
129 age is corrected after deducting the carbon pool. Otherwise, the influence of carbon pool is not
130 considered. The age-depth model for the pollen records was estimated by linear interpolation
131 between adjacent available dates or by regression. Using ranking schemes from the Cooperative
132 Holocene Mapping Project, the quality of dating control for the mid-Holocene was assessed by
133 assigning a rank from 1 to 7. 70% of the records used in our study fell into the first and second
134 classes (see Table 1 for detailed information) according to the Webb 1-7 standards (Webb, III
135 T., 1985). Vegetation type was quantitatively reconstructed using biomization (Prentice et al.,
136 1996), following the classification of plant functional types (PFTs) and biome assignment in
137 China by the Members of China Quaternary Pollen Data (CQPD, 2000), which has been widely
138 tested in surface sediment. The new sites (91 digitized data and three original data) added to
139 our database improved the spatial coverage of pollen records, especially in the northwest, the
140 Tibetan Plateau, the Loess Plateau and southern regions, where the data in the previous
141 databases are very limited.

142 Modern monthly mean climate variables investigated in this study, including temperature,
143 precipitation and cloudiness (total cloud fraction), have been collected for each modern pollen
144 site based on the datasets (1951-2001) from 657 meteorological observation stations over
145 China (China Climate Bureau, China Ground Meteorological Record Monthly Report, 1951-
146 2001). The MH soil properties and characteristics used in the inverse vegetation model were
147 kept the same with PI conditions, which are derived from the digital world soil map produced

148 by the Food and Agricultural organization (FAO) (FAO, 1995). Atmospheric CO_2
149 concentration for the MH was taken from ice core records (EPICA community members
150 2004), and was set at 270 ppmv.

151 A 3-layer back-propagation (BP) artificial neural network technique (ANN) was used for
152 interpolation on each pollen site (Caudill and Butler, 1992). Five input variables (latitude,
153 longitude, elevation, annual precipitation, annual temperature) and one output variable (biome
154 scores) have been chosen in ANN for the modern vegetation. The ANN has been calibrated
155 on the training set, and its performance has been evaluated on the verification set (20%,
156 randomly extracted from the total sets). After a series of training run, the lowest verification
157 error is obtained with 5 neurons in the hidden layer after 10000 iterations. In our study, at
158 each pollen site, we firstly applied the biomization method to get the biome scores for both
159 present-day and MH. The anomalies between past (6 ka) and modern vegetation indices
160 (biome scores) was then interpolated to the 0.2×0.2° grid resolution by applying the ANN.
161 After that, the modern grid values are added to the values of the grid of palaeo-anomalies to
162 provide gridded paleo-biome indices. Finally, the biome with the highest index is attributed to
163 each grid point. This ANN method is more efficient than many other techniques on the
164 condition that the results are validated by independent data sets, and therefore, it has been
165 widely applied in paleoclimatology (Guiot et al., 1996; Peyron et al., 1998). The schematic
166 diagram of ANN (Figure S1) can be found in Supplementary Information.

167 **2.2 Climate models**

168 PMIP, a long-standing initiative, is a climate-model evaluation project which provides an
169 efficient mechanism for using global climate models to simulate climate anomalies for past
170 periods and to understand the role of climate feedbacks. In its third phase (PMIP3, Braconnot
171 et al., 2011), the models were identical to those used in the Climate Modelling Intercomparison
172 Project 5 (CMIP5) experiments. The experimental set-up for the mid-Holocene simulations in

PMIP3 followed the PMIP protocol (Taylor et al., 2012, https://wiki.lsce.ipsl.fr/pmip3/doku.php/pmip3:design:6k:final). The main forcing between the MH and PI in PMIP3 is the change in the orbital configuration. More precisely, the orbital configuration in the MH climate has an increased summer insolation and a decreased winter insolation in the Northern Hemisphere compared to the PI climate (Berger, 1978). In addition, the CH_4 concentration is prescribed at 650 ppbv in the MH, while it is set at 760 ppbv in PI (Table 2).

All 13 models (Table 3) from PMIP3 that have the MH simulation have been included in our study, including eight atmosphere-ocean (AO) models and five atmosphere-ocean-vegetation (AOV) models. Means for the last 30 years were calculated from the archived time-series data on individual model grids for climate variables. Then the near surface temperature and precipitation flux, were bi-linearly interpolated to a uniform 2.5° grid, in order to compute the bioclimatic variables (e.g. MAT, MAP, MTWM, MTCO, July precipitation) onto a common grid for comparison with the reconstruction results.

2.3 Vegetation model

The vegetation model, BIOME4 is a coupled bio-geography and biogeochemistry model developed by Kaplan et al. (2003). Monthly mean temperature, precipitation, sunshine percentage (an inverse measure of cloud area fraction), absolute minimum temperature, atmospheric CO_2 concentration and subsidiary information about the soil's physical properties like water retention capacity and percolation rates are the main input variables. It represents 13 plant functional types (PFTs), which have different bioclimatic limits. The PFTs are based on physiological attributes and bioclimatic tolerance limits such as heat, moisture and chilling requirements and resistance of plants to cold. These limits determine the areas where the PFTs can grow in a given climate. A viable combination of these PFTs defines a particular biome among 28 potential options. These 28 biomes can be further classified into 8 megabiomes

198 (Table S1). BIOME4 has been widely utilized to analyze the past, present and potential future
199 vegetation patterns (e.g. Bigelow et al., 2003; Diffenbaugh et al., 2003; Song et al., 2005). In
200 this study, we conducted 13 PI and associated MH biome simulations using PMIP3 climate
201 fields (temperature, precipitation and sunshine) as inputs. The climate fields, obtained from
202 PMIP3, are the monthly mean data of the last 30 model years.

203 **2.4 Statistics and interpolation for vegetation distribution**

204 To quantify the differences between simulated (based on BIOME4 forced by the climate
205 model output) and reconstructed (from pollen) megabiomes, a map-based statistic (point-to-
206 point comparison with observations) called ΔV（Sykes et al., 1999; Ni et al., 2000）was applied
207 to our study. ΔV is based on the relative abundance of different plant life forms (e.g. trees, grass,
208 bare ground) and a series of attributes (e. g. evergreen, needle-leaf, tropical, boreal) for each
209 vegetation class. The definitions and attributes of each plant form follow naturally from the
210 BIOME4 structure and the vegetation attribute values in the ΔV computation were defined for
211 BIOME4 in the same way as for BIOME1（Sykes et al., 1999). The abundance and attribute
212 values are given in Table 4 and Table 5, which describe the typical floristic composition of the
213 biomes. Weighting the attributes is subjective because there is no obvious theoretical basis for
214 assigning relative significance. Transitions between highly dissimilar megabiomes have a
215 weighting of close to 1, whereas transitions between less dissimilar megabiomes are assigned
216 smaller values. The overall dissimilarity between model and data megabiome maps was
217 calculated by averaging the ΔV for the grids with pollen data, while the value was set at 0 for
218 any grid without data. ΔV values < 0.15 can be considered to point to very good agreement
219 between simulated and actual distributions, 0.15-0.30 is good, 0.30-0.45 is fair, 0.45-0.60 is
220 poor, and > 0.80 is very poor (adjusted from Zhang et al., 2010).

2.5 Inverse vegetation model

The Inverse Vegetation Model (Guiot et al., 2000; Wu et al., 2007), highly dependent on the BIOME4 model, is applied to our reconstruction. The key concept of this model can be summarized in two points: firstly, a set of transfer functions able to transform the model output into values directly comparable with pollen data is defined. There is not full compatibility between the biome typology of BIOME4 and the biome typology of pollen data. A transfer matrix (Table S2) was defined in our study where each BIOME4 vegetation type is assigned a vector of values, one of each pollen vegetation type, ranging from 0 (representing an incompatibility between BIOME4 type and pollen biome type) to 15 (corresponding to a maximum compatibility). Secondly, using an iterative approach, a representative set of climate scenarios compatible with the vegetation records is identified within the climate space, constructed by systematically perturbing the input variables (e.g. ΔT, ΔP) of the model (Table S3).

The Inverse Vegetation Model (IVM) provides a possibility, for the first time, to reconstruct both annual and seasonal climates for the MH over China. Moreover, it offers a way to consider the impact of CO_2 concentration on competition between PFTs as well as on the relative abundance of taxa, and thus make the reconstructions from pollen records more reliable. More detailed information about IVM can be found in Wu et al. (2007).

We applied the inverse model to modern pollen samples to validate the approach by reconstructing the modern climate at each site and comparing it with the observed values. The high correlation coefficients (R=0.75–0.95), intercepts close to 0 (except for the mean temperature of the warmest month), and slopes close to 1 (except for the July precipitation) demonstrated that the inversion method worked well for most variables in China (see Table 6).

2.6 Sensitivity test for vegetation feedback

To quantify the vegetation feedback on climate change during mid-Holocene over China, we performed a sensitivity test using CESM version 1.0.5. This version, developed at the National Center for Atmospheric Research, is a widely used coupled model with dynamic atmosphere (CAM4), land (CLM4), ocean (POP2), and sea-ice (CICE4) components (Gent et al., 2011). Here, we use ~2° resolution for CAM4(~1.9° for latitudes × 2.5° for longitudes) in the horizontal direction and 26 layers in the vertical direction. The POP2 adopts a finer grid, with a nominal 1° horizontal resolution and 60 layers in the vertical direction. The land and sea-ice components have the same horizontal grids as the atmosphere and ocean components, respectively.

Two experiments were conducted, including a mid-Holocene (MH) experiment (6 ka) with original vegetation setting (prescribed as PI vegetation for MH) and a MH experiment with reconstructed vegetation (6 ka_VEG). In detail, experiment 6 ka used the MH orbital parameters (Eccentricity=0.018682; Obliquity=24.105°; Longitude of the perihelion =0.87°) and modern vegetation (Salzmann et al., 2008). Compared to experiment 6 ka, experiment 6 ka_VEG used our reconstructed vegetation in China. Except for the changed vegetation, all other boundary conditions were kept unchanged in these two experiments, including the solar constant (1365 W m^{-2}), modern topography and ice sheet, and pre-industrial greenhouse gases (CO_2 = 280 ppmv; CH_4 = 760 ppbv; N_2O = 270 ppbv). Experiment 6 ka was initiated from the default pre-industrial simulation and run for 500 model years. Experiment 6 ka_VEG was initiated from model year 301 of experiment 6 ka and run for another 200 model years. We analyzed the computed climatological means of the last 50 model years from each experiment here.

3. Results

3.1 Comparison of annual and seasonal climate changes at the MH

In this study, we collected 159 pollen records, broadly covering the whole of China (Fig. 1). To check the reliability of the collected data, we first categorized our pollen records into megabiomes in line with the standard tables developed for the BIOME6000 (Table S1), and compared them with the BIOME6000 dataset (Fig.2). The match between collected data and the BIOME6000 is more than 90% (145 out of 159 sites) for both the MH and PI.

Based on pollen records, the spatial pattern of climate changes over China during the MH, deduced from IVM, are presented in Fig. 3 (left panel, points), alongside the results from PMIP3 models (shaded in Fig. 3). For temperature, a warmer-than-present annual climate condition (~0.7 K on average) is derived from pollen data (the points in Fig. 3a), with the largest increase occurring in the northeast (3-5 K) and a decrease in the northwest and on Tibetan Plateau. On the other hand, the results from a multi-model ensemble (MME) indicate a colder annual temperature generally (~-0.4 K on average), with significant cooling in the south and slight warming in the northeast (shaded in Fig. 3a). Of the 13 models, 11 simulate a cooler annual temperature compared with PI as MME. However, two models (HadeGEM2-ES and CNRM-CM5) present the same warmer condition as was found in the reconstruction (Fig. 3d). Compared to the reconstruction, the annual mean temperature during the MH is largely underestimated by most PMIP3 models, which depict an anomaly ranging from ~-1 to ~0.5 K. Concerning seasonal change, during the MH, MTWA from the data is ~0.5 K higher than PI, with the largest increase in the northeast and a decrease in the northwest. From model outputs, an average increase of ~1.2 K is reproduced by MME, with a more pronounced warming at high latitudes which is consistent with the insolation change (Berger, 1978). Fig. 3e shows that all 13 models reproduce the same warmer summer temperatures as the data, and that

HadGEM2-ES and CNRM-CM5, reproduce the largest increases among the models. Although models simulate warmer MTWA, which is consistent with reconstructions, there is a discrepancy between them on MTCO. In Fig. 3c, the data show an overall increase of ~1 K, with the largest increase occurring in the northeast and a decrease of opposite magnitude on the Tibetan Plateau. Inversely, MME reproduces a decreased MTCO with an average amplitude of ~-1.3 K, the areas with strongest cooling being the southeast, the Loess Plateau and the northwest. Similarly to the MME, all 13 models simulate a colder-than-present climate with amplitudes ranging from ~-2.0 K (CCSM4 and FGOALS-g2) to ~-0.7 K (HadGEM2-ES and CNRM-CM5).

Concerning the annual change in precipitation, the reconstruction shows wetter conditions during the MH across almost the whole of China with the exception of part of the northwest. The southeast presents the largest increase in annual precipitation. All but 2 models (MIROC-ESM and FGOALS-g2) depict wetter conditions with an amplitude of ~10 mm to ~50 mm. The reconstruction and MME results also indicate an increased annual precipitation during MH (Fig.4a), with a much larger magnitude visible in the reconstruction (~30 mm, ~230 mm respectively). The main discrepancy in annual precipitation between simulations and reconstruction occurs in the northeast, which is depicted as drier by the models and wetter by the data. With regard to seasonal change, the reconstruction shows an overall increase in July rainfall (~50 mm on average), with a decrease in the northwestern regions and East Monsoon region at Yangtze River valley. In line with the reconstruction, the MME also shows an overall increase in rainfall (~7 mm on average), with a decrease in the northwest for July (Fig.4b). Notably, a much larger increase is simulated for the south and the Tibetan Plateau by the models, while the opposite pattern emerges along the eastern margin from both models and data. For January precipitation, the reconstruction shows an overall increase in most region (~15 mm), except for the northwestern region, while MME indicates a slight decrease (~3 mm on average).

More detailed information about the geographic distribution of simulated temperature and precipitation for each model can be found in Fig. S2-S7.

Table S4 provides the biome score from IVM for pollen data collected from published papers. The reconstructed climate change derived from IVM at each pollen site can be found in Table S5, in which the columns show the median and the 90% interval (5th to 95th percentage) for feasible climate values produced with the IVM approach. The simulated values for each of the climate variables as shown in the boxplots (Figure 3 and Figure 4) are given in the Table S6 and Table S7. All the values mentioned above are the mean of the values at 159 pollen sites.

3.2 Comparison of vegetation change at the MH

The use of the PMIP3 database is clearly limited by the different vegetation inputs among the models for the MH period (Table S8). Only HadGEM2-ES and HadGEM2-CC use a dynamic vegetation for the MH, and the vegetation of the other 11 models are prescribed to PI with or without interactive LAI, which can introduce a bias to the role of vegetation-atmosphere interaction in the MH climates. To evaluate the model results against the reconstruction for the MH vegetation, we conducted 13 biome simulations with BIOME4 using the PMIP3 climate fields, and the megabiome distribution for each model during the MH is displayed in Fig. 5 (see Fig. S8 for a comparison of PI biomes). To quantify the model-data dissimilarity between megabiomes, a map-based statistic called ΔV（Sykes et al., 1999; Ni et al., 2000) was applied here (cf. Section 2.4).

Fig. S9 shows the dissimilarity between simulations and observations for megabiomes during the MH, with the overall values for ΔV ranging from 0.43 (HadGEM2-ES) to 0.55 (IPSL-CM5A-LR). According to the classification of ΔV (cf. Section 2.4) for the 13 models, 12 (all except HadGEM2-ES) showed poor agreement with the observed vegetation distribution. Most models poorly simulate the desert, grassland and tropical forest areas for both periods, but

perform better for warm mixed forest, tundra and temperate forest. However, this statistics is based on a point-to-point comparison and so the ΔV calculated here cannot represent an estimation of full vegetation simulation due to the uneven distribution of pollen data and the potentially huge difference in area of each megabiome. For instance, tundra in our data for PI is represented by only 4 points, which counts for a small contribution to the ΔV since we averaged it over a total of 159 points, but this calculation could induce a significant bias if these 4 points are representative of a large area of China.

So, we used the biome scores based on the artificial neural network technique as described by Guiot et al. (1996) for interpolation (the plots in red rectangle in Fig. 5), and compared the simulated vegetation distribution from BIOME4 for each model with the interpolated pattern. During the MH, most models are able to capture the tundra on the Tibetan Plateau as well as the combination of warm mixed forest and temperate forest in the southeast. However, all models fail to simulate or underestimate the desert area in the northwest compared to reconstructed data. The main model-data inconsistency in the MH vegetation distribution occurs in the northeast, where data show a mix of grassland and temperate forest, and the models show a mix of grassland and boreal forest.

The area statistics carried out for simulated vegetation changes (Fig. 6) reveals that the main difference during the MH, compared with PI, is that grassland replaced boreal forest in large tracts of the northeast (Fig. 5, Fig. S8). No other significant difference in vegetation distribution between the two periods was derived from models. Unlike in models, three main changes in megabiomes during the MH are depicted by the data. Firstly, the megabiomes converted from grassland to temperate forest in the northeast. Secondly, a large area of temperate forest was replaced in the southeast by a northward expansion of warm mixed forest. Thirdly, in the northwest and at the northern margin of the Tibetan Plateau, part of the desert area changed into grassland. However, none of the models succeed in capturing these features, especially the

transition from grassland into forest in the northeast during the MH. Therefore, this failure to capture vegetation changes between the two periods will lead to a cumulating inconsistency in the model-data comparison for climate anomalies because if these computed vegetation were used as boundary conditions in MH climate simulations.

4. Discussion

4.1 Validation and uncertainties of the reconstructions

To investigate the discrepancy between model and reconstructions for the MH climate change over China, the reliability of our reconstruction should be first considered. We therefore compared our reconstruction with previous studies concerning the MH climate change over China based on multiple proxies (including pollen, lake core, palaeosol, ice core, peat and stalagmite), the related references and detailed information are listed in Supplementary Information (Table S9 and Table S10). In comparison with PI conditions, most reconstructions reproduced warmer and wetter annual condition during the MH (Fig. 7), as in our study. In other words, this model-data discrepancy for climate change over China during the MH is common and robust w.r.t. reconstructions derived from different proxies. Our study reinforces the picture given by the discrepancies between PMIP simulations and pollen data based on a synthesis of the literature.

However, there could still be some biases due to the reconstruction method. Estimated climates for the present day from IVM were compared with observed climates (Table 6). The slopes and intercepts show a slight bias for annual and January precipitation, while there is a larger bias between IVM reconstruction and observation for temperature and July precipitation. IVM relies heavily on BIOME4, and since BIOME4 is a global vegetation model, it is possible that the spatial robustness of regional reconstruction could be less than that of global reconstruction due to the failure in simulating local features (Bartlein et al., 2011). Moreover,

the output of the model cannot be directly compared to the pollen data, the conversion of BIOME4 biomes to pollen biomes by the transfer matrix may add the source of uncertainty in reconstruction. All these biases in reconstruction should be considered in the evaluation of the discrepancy between model and data for climate change during the MH over China.

4.2 Uncertainties for simulations

The discrepancies between model and data for MH climate change can also result from uncertainties in simulation and/or model characteristics. First, the coarse spatial resolution of models can be a factor of discrepancy: previous studies show that the GCMs from PMIP3 are reliable to simulate the geographical distribution of temperature and precipitation over China for present day. However, compared with observation, most models have topography-related cold biases (Jiang et al., 2016). The climate fields, directly used from the model output without downscaling, will not contain the spatial variability of modern climate that in topographically complex areas. Thus, it is necessary to check to which degree the model-data mismatch is related to rough topography used in the climate models. In PMIP3, MRI-CGCM3 has the highest resolution (Atmosphere: 320*160*L48; Ocean: 364*368*L51), while IPSL-CM5A-LR has the lowest one (Atmosphere: 96*96*L39; Ocean: 182*149*L31). In Fig. 8, we give the actual modern topography and the interpolated topography used in MRI-CGCM3 and IPSL-CM5A-LR. For MRI-CGCM3, the topography is very close to the observation, so for this model, the model-data discrepancy during MH over China is not related to the resolution. However, for the model with coarse resolution (IPSL-CM5A-LR), it is true that the coarse version of model will lead to bias in topography when the regional diversity is discussed. The spatial variations in topography could influence the vegetation and hence the simulated climate. To quantify this impact, we compare the topography and PI climate results of IPSL-CM5A-LR and IPSL-CM5A-MR. Fig. 9 shows that the difference in topography caused by model resolution does have an impact on small scales (e.g. south region of the Tibetan Plateau), not on the overall

pattern. But those small or regional-scale variations in climate can have a large impact on vegetation and hence reconstructed climate. For a better comparison, in the future work, downscaled climate variables should be considered.

Secondly, besides the qualitative consistency among models, caused by the protocol of PMIP3 experiments (Table 2), a variability in the magnitude of anomalies between models is clearly illustrated by the boxplots (Fig.3 and Fig.4), especially for the temperature anomaly. Fig. S10 demonstrates that there is no clear relationship between PI temperature and temperature anomaly (MH-PI). In other words, these disparities in value or even pattern among models do not related to the difference in PI simulations in a simple manner, instead, they reflect the obvious differences in the response by the climate models to the MH forcing, which raises on the question of the magnitude of feedbacks among models.

As positive feedbacks between climate and vegetation are important to explain regional climate changes, the failure of the models to represent the amplitude and pattern of the observed vegetation differences (see Section 3.2) could amplify and partly account for the model-data disparities in climate change, mainly due to variations in the albedo. Because the HadGEM2-ES and HadGEM2-CC are the only two models in PMIP3 with dynamic vegetation simulation for the MH, we focused on these models to examine the variations in vegetation fraction in the simulations. The main vegetation changes during the MH demonstrated by HadGEM2-ES are increased tree coverage (~15%) and a decreased bare soil fraction (~6%), while HadGEM2-CC depicts a ~3% decrease in tree fraction and a ~1% increase in bare soil (Fig. S11). We made a rough calculation of albedo variance caused solely by vegetation change for both two models and for our reconstruction, based on the area fraction and albedo value of each vegetation type (Betts, 2000; Bonfils et al., 2001; Oguntunde et al., 2006; Bonan, 2008). The overall albedo change from the vegetation reconstruction during the MH shows a ~1.8% decrease when snow-free, with a much larger impact (~4.2% decrease) when snow-covered. The results from

HadGEM2-ES are highly consistent with the albedo changes from the reconstruction, featuring a ~1.4% (~6.5%) decrease without (with) snow, while HadGEM2-CC produces an increased albedo value during the MH (~0.22% for snow-free, ~1.9% with snow-cover), depending on its vegetation simulation. Two ideas could be inferred from this calculation, 1) HadGEM2-ES is much better in simulating the MH vegetation changes than HadGEM2-CC. 2) the failure by models to capture these vegetation changes will result in a much larger impact on winter albedo (with snow) than summer albedo (without snow). In conclusion, there is an obvious advantage of using AOVGCM instead of AOGCM when we discussing about the MH climate, but the premise is that the AOVGCM can simulate accurate vegetation distribution.

These surface albedo changes due to vegetation changes could have a cumulative effect on the regional climate by modifying the radiative fluxes. For instance, the spread of trees into the grassland biome in the northeast during the MH, revealed by the reconstruction in our study, should act as a positive feedback to climate warming by increasing the surface net shortwave radiation associated with reductions in albedo due to taller and darker canopies (Chapin et al., 2005). Previous studies show that cloud and surface albedo feedbacks on radiation are major drivers of differences between model outputs for past climates. Moreover, the land surface feedback shows large disparities among models (Braconnot and Kageyama, 2015).

We used a simplified approach (Taylor et al., 2007) to quantify the feedbacks and to compare model behavior for the MH, thus justifying the focus on surface albedo and atmospheric scattering (mainly accounting for cloud change). Surface albedo and cloud change are calculated using the simulated incoming and outgoing radiative fluxes at the Earth's surface and at the top of atmosphere (TOA), based on data for the last 30 years averaged from all models. Using this framework, we quantified the effect of changes in albedo on the net shortwave flux at TOA (Braconnot and Kageyama, 2015), and further investigated the relationship between these changes and temperature change. Fig.10 shows that most models produced a negative

cloud cover and surface albedo feedback on the annual mean shortwave radiative forcing. Concerning seasonal change, the shortwave cloud and surface feedback in most models tend to counteract the insolation forcing during the boreal summer, while they enhance the solar forcing during winter. A strong positive correlation between albedo feedback and temperature change is depicted, with a large spread in the models owing to the difference in albedo in the 13 models. In particular, CNRM-CM5 and HadGEM2-ES capture higher values of cloud and surface albedo feedback, which could be the reason for the reversal of the decreased annual temperature seen in other models (Fig. 3d).

However, the vegetation patterns produced by BIOME4 in Figure 5 are not used in PMIP3 experiment setup. They are onlydetermined by the input variables from models. Therefore, the disagreements of MH vegetation pattern are possibly inherited from the PI. To better quantify the vegetation-climate feedback, two experiments were conducted in CESM version 1.0.5, including a mid-Holocene (MH) experiment (6 ka) with original vegetation setting (prescribed as PI vegetation for the MH) and a MH experiment with reconstructed vegetation (6 ka_VEG). Fig. 11 shows the climate anomalies (6 ka_VEG minus 6 ka) between two simulations, for both annual and seasonal scale. For temperature, it is clear that the 6 ka_VEG simulation reproduces a warmer annual mean climate (~0.3 K on average) as well as an obviously warmer winter (~0.6 K on average). For precipitation, the reconstructed vegetation leads to more annual and seasonal precipitation, which can also reconcile the model-data discrepancy of increase amplitude for precipitation during the MH (data reproduced larger amplitude than model, revealed by our study). So the mismatch between model and data in MH vegetation could partly account for the discrepancy of climate due to the interaction between vegetation and climate through radiative and hydrological forcing with albedo. These results highlight the value of building a new generation of models able to capture not only the

atmosphere and ocean response, but also the non-linear responses of vegetation and hydrology to climate change.

5. Conclusion

In this study, we compare the annual and seasonal outputs from the PMIP3 models with an updated synthesis of climate reconstructions over China, including, for the first time, the seasonal cycle of temperature and precipitation. In response to the seasonal insolation change prescribed in PMIP3 for the MH, all models produce similar large-scale patterns for seasonal temperature and precipitation (higher than present July precipitation and MTWA, lower than present MTCO). The main discrepancy emerging from the model-data comparison occurs for the mean annual temperature and MTCO, where data show an increased value and most models simulate the opposite except CNRM-CM5 and HadGEM2-ES that reproduced the higher-than-present MH annual temperature. By conducting simulations with BIOME4 and CESM, we show that surface processes are the key factors explaining the discrepancies between models and data. These results show the importance of including the non-linear responses of the surface water and energy balance related to vegetation changes. However, it should also be noted that prescribing the vegetation with reconstructed biomes would reduce the power of the biome-based climate reconstruction, owing to the potential circularity (prescribe the vegetation to get the vegetation). Moreover, besides the vegetation influence, to the impact of rough topography, soil type and other possible factors on model-data discrepancy remains to be investigated in future work.

Data availability

The PMIP3 output is publicly available on the PMIP website (http://pmip3.lsce.ipsl.fr/) . The 65 pollen biomization results are provided by Members of China Quaternary Pollen Data Base

(CQPD), Table 1 shows the information (including references) of the 91 collected pollen records and 3 original ones in our study, the biome scores of these 94 pollen records derived from IVM are listed in Table S4, and the digitized data of pollen can be requested to Qin Li (liqin@mail.iggcas.ac.cn). All the reconstructed climate values at each pollen site from IVM are provided in Table S5. For the data from CQPD, the basic information (location, data supporter, age control and biome type of each site) can be found in CQPD (2000), while the original data are not publicly available yet. These data can be requested to Yunli Luo (lyl@ibcas.ac.cn, Institute of Botany, Chinese Academy of Sciences, Beijing, 100093, China), a core member and academic secretary of the CQPD.

Author contribution

Yating Lin carried out the model-data analysis and prepared the first manuscript, Gilles Ramstein contributed a lot to the paper's structure and content, Haibin Wu provided the reconstruction results from IVM and contributed the paper's structure and content. Raj Rani-Singh conducted the BIOME4 simulations. Ran Zhang carried out the simulation in CESM. Pascale Braconnot, Masa Kegeyama and Zhengtang Guo contributed great ideas on model-data comparison work. Qin Li and Yunli Luo provided pollen data. All co-authors helped to improve the paper.

Competing interest

The authors declare no competing interests.

Acknowledgements

We acknowledge the Paleoclimate Modeling Intercomparison Project and World Climate Research Program's Working Group on Coupled Modelling, which is responsible for PMIP/CMIP, and we thank the climate modelling groups for producing and making available their model output. We are grateful to Marie-France Loutre, Patrick Bartlein and three

anonymous reviewers for constructive comments. This research was funded by the National Basic Research Program of China (Grant no. 2016YFA0600504), the National Natural Science Foundation of China (Grant nos. 41572165, 41690114, and 41125011), the Sino-French Caiyuanpei Program, the Bairen Programs of the Chinese Academy of Sciences, and the JPI-Belmont PACMEDY project (Grant no. ANR-15-JCLI-0003-01). We also acknowledge Labex L-IPSL, funded by the French Agence Nationale de la Recherche (Grant #ANR-10-LABX-0018) for its support to the biome modelling based on the PMIP database.

References

An, C., Zhao, J., Tao, S., Lv, Y., Dong, W., Li, H., Jin, M., and Wang, Z.: Dust variation recorded by lacustrine sediments from arid Central Asia since ~ 15 cal ka BP and its implication for atmospheric circulation, Quaternary Research, 75, 566-573, 2011.

Bao, Q., Lin, P., Zhou, T., Liu, Y., Yu, Y., Wu, G., He, B., He, J., Li, L., Li, J., Li, Y., Liu, H., Qiao, F., Song, Z., Wang, B., Wang, J., Wang, P., Wang, X., Wang, Z., Wu, B., Wu, T., Xu, Y., Yu, H., Zhao, W., Zheng, W., and Zhou, L.: The flexible global ocean-atmosphere-land system model, spectral version 2: FGOALS-s2. Advances in Atmospheric Sciences, 30, 561-576, 2013.

Bartlein, P. J., Harrison, S. P., Brewer, S., Connor, S., Davis, B. A. S., Gajewski, K., Guiot, J., Harrison-Prentice, T. I., Henderson, A., Peyron, O., Prentice, I. C., Scholze, M., Seppä, H., Shuman, B., Sugita, S., Thompson, R. S., Viau, A. E., Williams, J., and Wu, H.B.: Pollen-based continental climate reconstructions at 6 and 21ka: a global synthesis, Climate Dynamics, 37, 775-802, 2011.

Berger, A.: Long-Term Variations of Daily Insolation and Quaternary Climatic Changes, Journal of the Atmospheric Sciences, 35, 2362-2367, 1978.

560 Betts, R. A.: Offset of the potential carbon sink from boreal forestation by decreases in
561 surface albedo, Nature, 408, 187-190, 2000.

562 Bigelow, N. H., Brubaker, L. B., Edwards, M. E., Harrison, S. P., Prentice, I. C., Anderson, P.
563 M., Andreev, A. A., Bartlein, P. J., Christensen, T. R., Cramer, W., Kaplan, J. O.,
564 Lozhkin, A. V., Matveyeva, N. V., Murray, D. F., David McGuire, A., Razzhivin, V. Y.,
565 Ritchie, J. C., Smith, B., Walker, A. D., Gajewski, K., Wolf, V., Holmqvist, B. H.,
566 Igarashi, Y., Kremenetskii, K., Paus, A., Pisaric, M. F. J., and Volkova, V. S.: Climate
567 change and Arctic ecosystems: 1. Vegetation changes north of 55°N between the last
568 glacial maximum, mid-Holocene and present, Journal of Geophysical Research, 108, 1-
569 25, 2003.

570 Bonan, G. B.: Forests and Climate Change: Forcings, Feedbacks, and the Climate Benefits of
571 Forests, Science, 320, 1444-1449, 2008.

572 Bonfils, C., de Noblet-Ducoudré, N, Braconnot, P., and Joussaume, S.: Hot Desert Albedo
573 and Climate Change: Mid-Holocene Monsoon in North Africa, Journal of Climate, 14,
574 3724–3737, 2001.

575 Braconnot, P., and Kageyama, M.: Shortwave forcing and feedbacks in Last Glacial
576 Maximum and Mid-Holocene PMIP3 simulations, Philosophical Transactions of the
577 Royal Society A: Mathematical, Physical and Engineering Sciences, 373, 2054-2060,
578 2015.

579 Braconnot, P., Harrison, S. P., Kageyama, M., Bartlein, P. J., Masson-Delmotte, V., Abe-
580 Ouchi, A., Otto-Bliesner, B., and Zhao, Y.: Evaluation of climate models using
581 palaeoclimatic data: Nature Climate Change, 2, 417-421, 2012.

582 Braconnot, P., Otto-Bliesner, B., Harrison, S., Joussaume, S., Peterchmitt, J. Y., Abe-Ouchi,
583 A., Crucifix, M., Driesschaert, E., Fichefet, T., Hewitt, C. D., Kageyama, M., Kitoh, A.,

584 Laine, A., Loutre, M. F., Marti, O., Merkel, U., Ramstein, G., Valdes, P., Weber, S. L.,
585 Yu, Y., and Zhao, Y.: Results of PMIP2 coupled simulations of the Mid-Holocene and
586 Last Glacial Maximum-Part 1: experiments and large-scale features, Climate of the Past,
587 3, 261-277, 2007a.

588 Braconnot, P., Otto-Bliesner, B., Harrison, S., Joussaume, S., Peterschmitt, J. Y., Abe-Ouchi,
589 A., Crucifix, M., Driesschaert, E., Fichefet, T., Hewitt, C. D., Kageyama, M., Kitoh, A.,
590 Loutre, M. F., Marti, O., Merkel, U., Ramstein, G., Valdes, P., Weber, L., Yu, Y., and
591 Zhao, Y.: Results of PMIP2 coupled simulations of the Mid-Holocene and Last Glacial
592 Maximum-Part 2: feedbacks with emphasis on the location of the ITCZ and mid- and high
593 latitudes heat budget, Climate of the Past, 3, 279-296, 2007b.

594 Cai, Y.: Study on environmental change in Zoige Plateau: Evidence from the vegetation
595 record since 24000a B.P., Chinese Academy of Geological Sciences, Mater Dissertation,
596 2008 (in Chinese with English abstract).

597 Caudill, M., Bulter, C.: Understanding Neural Networks, Basic Networks, 1, 309, 1992.

598 Chapin, F. S., Sturm, M., Serreze, M. C., McFadden, J. P., Key, J. R., Lloyd, A. H.,
599 McGuire, A. D., Rupp, T. S., Lynch, A. H., Schimel, J. P., Beringer, J., Chapman, W. L.,
600 Epstein, H. E., Euskirchen, E. S., Hinzman, L. D., Jia, G., Ping, C.L., Tape, K. D.,
601 Thompson, C. D. C., Walker, D. A., and Welker, J. M.: Role of Land-Surface Changes in
602 Arctic Summer Warming, Science, 310, 657-660, 2005.

603 Chen, F., Cheng, B., Zhao, Y., Zhu, Y., and Madsen, D. B.: Holocene environmental change
604 inferred from a high-resolution pollen record, Lake Zhuyeze, arid China, The Holocene,
605 16, 675-684, 2006.

606 Chen, F., Xu, Q., Chen, J., Birks, H. J. B., Liu, J., Zhang, S., Jin, L., An, C., Telford, R. J.,
607 Cao, X., Wang, Z., Zhang, X., Selvaraj, K., Lu, H., Li, Y., Zheng, Z., Wang, H., Zhou, A.,
608 Dong, G., Zhang, J., Huang, X., Bloemendal, J., and Rao, Z.: East Asian summer
609 monsoon precipitation variability since the last deglaciation, Scientific Reports, 5, 1-11,
610 2015.

611 Cheng, B., Chen, F., and Zhang, J.: Palaeovegetational and Palaeoenvironmental Changes in
612 Gonghe Basin since Last Deglaciation, Acta Geographica Sinica, 11, 1336-1344, 2010 (in
613 Chinese with English abstract).

614 Cheng, H., Edwards, R. L., Sinha, A., Spötl, C., Yi, L., Chen, S., Kelly, M., Kathayat, G.,
615 Wang, X., Li, X., Kong, X., Wang, Y., Ning, Y., and Zhang, H.: The Asian monsoon over
616 the past 640,000 years and ice age terminations, Nature, 534, 640, 2016.

617 Cheng, Y.: Vegetation and climate change in the north-central part of the Loess Plateau since
618 26,000 years, China University of Geosciences, Master Dissertation, 2011 (in Chinese
619 with English abstract).

620 Collins, W. J., Bellouin, N., Doutriaux-Boucher, M., Gedney. N., Halloran, P., Hinton, T.,
621 Hughes, J., Jones, C.D., Joshi, M., Liddicoat, S., Martin, G., O'Connor, F., Rae, J., Senior,
622 C., Sitch, S., Totterdell, I., Wiltshire, A., and Woodward, S.: Development and evaluation
623 of an Earth-system model—HadGEM2, Geoscientific Model Development, 4, 1051–1075,
624 2011.

625 Cui, M., Luo, Y., and Sun, X.: Paleovegetational and paleoclimatic changed in Ha'ni Lake,
626 Jilin since 5ka BP, Marine Geology & Quaternary Geology, 26, 117-122, 2006 (in
627 Chinese with English abstract).

628 Dallmeyer, A., Claussen, M., Ni, J., Cao, X., Wang, Y., Fischer, N., Pfeiffer, M., Jin, L.,
629 Khon, V., Wagner, S., Haberkorn, K., and Herzschuh, U.: Biome changes in Asia cinse

630 the mid-Holocene-and analysis of difference transient Earth system model simulations,
631 Climate of the Past, 13, 107-134, 2017.

632 Davis, B. A. S., Brewer, S., Stevenson, A. C., and Guiot, J.: The temperature of Europe
633 during the Holocene reconstructed from pollen data, Quaternary Science Reviews, 22,
634 1701-1716, 2003.

635 Diffenbaugh, N.S., Sloan, L.C., Snyder, M.A., Bell, J.L., Kaplan, J., Shafer, S.L., and
636 Bartlein, P.J.: Vegetation sensitivity to global anthropogenic carbon dioxide emissions in
637 a topographically complex region, Global Biogeochemical Cycles, 17, 1067,
638 doi:10.1029/2002GB001974, 2003.

639 Dufresne, J.L., Foujols, M.A., Denvil, S., Caubel, A., Marti, O., Aumont, O., Balkanski, Y.,
640 Bekki, S., Bellenger, H., Benshila, R., Bony, S., Bopp, L., Braconnot, P., Brockmann, P.,
641 Cadule, P., Cheruy, F., Codron, F., Cozic, A., Cugnet, D., Noblet, N., Duvel, J.P., Ethe,
642 C., Fairhead, L., Fichefet, T., Flavoni, S., Friedlingstein, P., Grandpeix, J.Y., Guez, L.,
643 Guilyardi, E., Hauglustaine, D., Hourdin, F., Idelkadi, A., Ghattas, J., Joussaume, S.,
644 Kageyama, M., Krinner, G., Labetoulle, S., Lahellec, A., Lefevre, M.-F., Lefevre, F.,
645 Levy, C., Li, Z.X., Lloyd, J., Lott, F., Madec, G., Mancip, M., Marchand, M., Masson, S.,
646 Meurdesoif, Y., Mignot, J., Musat, I., Parouty, S., Polcher, J., Rio, C., Schulz, M.,
647 Swingedouw, D., Szopa, S., Talandier, C., Terray, P., Viovy, N., and Vuichard, N.:
648 Climate change projections using the IPSL-CM5 Earth system model: from CMIP3 to
649 CMIP5, Climate Dynamics, 40, 2123-2165, 2013.

650 EPICA Community Members: Eight glacial cycles from an Antarctic ice core, Nature, 429,
651 623-628, 2004.

652 Food and Agricultural organization: Soil Map of the World 1:5000,000. 1995.

Farrera, I., Harrison, S. P., Prentice, I. C., Ramstein, G., Guiot, J., Bartlein, P. J., Bonnefille, R., Bush, M., Cramer, W., von Grafenstein, U., Holmgren, K., Hooghiemstra, H., Hope, G., Jolly, D., Lauritzen, S. E., Ono, Y., Pinot, S., Stute, M., and Yu, G.: Tropical climates at the Last Glacial Maximum: a new synthesis of terrestrial palaeoclimate data. I. Vegetation, lake-levels and geochemistry, Climate Dynamics, 15, 823-856, 1999.

Fischer, N., and Jungclaus, J. H.: Evolution of the seasonal temperature cycle in a transient Holocene simulation: orbital forcing and sea-ice, Climate of the Past, 7, 1139-1148, 2011.

Ganopolski, A., Kubatzki, C., Claussen, M., Brovkin, V., and Petoukhov, V.: The Influence of Vegetation-Atmosphere-Ocean Interaction on Climate during the Mid-Holocene, Science, 280, 1916-1919, 1998.

Gent, P.R., Danabasoglu, G., Donner, L.J., Holland, M.M., Hunke, E.C., Jayne, S.R., Lawrence, D.M., Neale, R.B., Rasch, P.J., Vertenstein, M., Worley, P.H., Yang, Z., and Zhang, M.: The community climate system model version 4, Journal of Climate, 24, 4973-4991, 2011.

Giorgetta, M.A., Jungclaus, J., Reick, C.H., Legutke, S., Bader, J., Bottinger, M., Brovkin, V., Crueger, T., Esch, M., Fieg, K., Glushak, K., Gayler, V., Haak, H., Hollweg, H.D., Ilyina, T., Kinne, S., Kornblueh, L., Matei, D., Mauritsen, T., Mikolajewicz, U., Mueller, W., Notz, D., Pithan, F., Raddatz, T.J., Rast, S., Redler, R., Roeckner, E., Schmidt, H., Schnur, R., Segschneider, J., Six, K.D., Stockhause, M., Timmreck, C., Wegner, J., Widmann, H., Wieners, K.H., Claussen, M., Marotzke, J., and Stevens, B.: Climate and carbon cycle changes from 1850 to 2100 in MPI-ESM simulations for the Coupled Model Intercomparison Project phase 5, Journal of Advances in Modeling Earth System, 5, 572-597, 2013.

676 Gong, X.: High-resolution paleovegetation reconstruction from pollen in Jiachuanyuan, Baoji,
677 Capital Normal University, Master Dissertation, 2006 (in Chinese with English abstract).

678 Guiot, J., and Goeury, C.: PPPBASE, a software for statistical analysis of paleoecological and
679 paleoclimatological data, Dendrochronologia, 14, 295-300, 1996.

680 Guiot, J., Harrison, S., and Prentice, I. C.: Reconstruction of Holocene precipitation patterns
681 in Europe using pollen and lake level data, Quaternary Research, 40, 139-149, 1993.

682 Guiot, J., Torre, F., Jolly, D., Peyron, O., Boreux, J. J., and Cheddadi, R.: Inverse vegetation
683 modeling by Monte Carlo sampling to reconstruct palaeoclimates under changed
684 precipitation seasonality and CO_2 conditions: application to glacial climate in
685 Mediterranean region, Ecological Modelling, 127, 119-140, 2000.

686 Guo, L., Feng, Z., Lee, X., Liu, L., and Wang, L.: Holocene climatic and environmental
687 changes recorded in Baahar Nuur Lake in the Ordos Plateau, Southern Mongolia of china,
688 Chinese Science Bulletin, 52, 959-966, 2007.

689 Hargreaves, J. C., Annan, J. D., Ohgaito, R., Paul, A., and Abe-Ouchi, A.: Skill and reliability
690 of climate model ensembles at the Last Glacial Maximum and mid-Holocene, Climate of
691 the Past, 9, 811-823, 2013.

692 Harrison, S. P., Bartlein, P. J., Brewer, S., Prentice, I. C., Boyd, M., Hessler, I., Holmgren, K.,
693 Izumi, K., and Willis, K.: Climate model benchmarking with glacial and mid-Holocene
694 climates, Climate Dynamics, 43, 671-688, 2014.

695 Harrison, S. P., Bartlein, P. J., K., Izumi, Li, G., Annan, J., Hargreaves, J., Braconnot, P., and
696 Kageyama, M.: Evaluation of CMIP5 paleo-simulations to improve climate projections,
697 Nature Climate Change, 5, 735-743, 2015.

698 Harrison, S., P., Braconnot, P., Hewitt, C., and Stouffer, R., J.: Fourth International Workshop
699 of the Palaeoclimate Modelling Intercomparison Project (PMIP): Lauching PMIP2 Phase
700 II, EOS, 83, 447-457, 2002.

701 Herzschuh, U., Kramer, A., Mischke, S., and Zhang, C.: Quantitative climate and vegetation
702 trends since the late glacial on the northeastern Tibetan Plateau deduced from Koucha
703 Lake pollen spectra, Quaternary Research, 71, 162-171, 2009.

704 Herzschuh, U., Kürschner, H., and Mischke, S.: Temperature variability and vertical
705 vegetation belt shifts during the last ~50,000 yr in the Qilian mountains (NE margin of
706 the Tibetan Plateau, China), Quaternary Research, 66, 133-146, 2006.

707 Huang, C., Elis, V. C., and Li, S.: Holocene environmental changes of Western and Northern
708 Qinghai-Xizang Plateau Based on pollen analysis, Acta Micropalaeontologica Sinica, 4,
709 423-432, 1996 (in Chinese with English abstract).

710 Jeffrey, S.J., Rotstayn, L.D., Collier, M., Dravitzki, S.M., Hamalainen, C., Moeseneder, C.,
711 Wong, K.K., and Syktus, J.I.: Australia' s CMIP5 submission using the CSIRO-Mk3.6
712 model, Australian Meteorological and Oceanographic Journal, 63, 1-13, 2013.

713 Jia, L., and Zhang, Y.: Studies on Palynological assemblages and paleoenvironment of late
714 Quaternary on the east margin of the Chanjiang (Yangtze) river delta, Acta
715 Micropalaeontologica Sinica, 23, 70-76, 2006 (in Chinese with English abstract).

716 Jiang, D., Lang, X., Tian, Z., and Wang, T.: Considerable Model–Data Mismatch in
717 Temperature over China during the Mid-Holocene: Results of PMIP Simulations, Journal
718 of Climate, 25, 4135-4153, 2012.

719 Jiang, D., Tian, Z., and Lang, X.: Mid-Holocene net precipitation changes over China: model-
720 data comparison, Quaternary Science Reviews, 82, 104-120, 2013.

721 Jiang, D., Tian, Z., and Lang, X.: Reliability of climate models for China through the IPCC
722 Third to Fifth Assessment Reports, International Journal of Climatology, 36, 1114-1133,
723 2016.

724 Jiang, Q., and Piperno., R. D.: Environmental and archaeological implications of a late
725 Quaternary palynological sequence, Poyang lake, Southern China, Quaternary Research,
726 52, 250-258, 1999.

727 Jiang, W., Guiot, J., Chu, G., Wu, H., Yuan, B., Hatté, C., and Guo, Z.: An improved
728 methodology of the modern analogues technique for palaeoclimate reconstruction in arid
729 and semi-arid regions, Boreas, 39, 145-153, 2010.

730 Jiang, W., Guo, Z., Sun, X., Wu, H., Chu, G., Yuan, B., Hatte, C., and Guiot, J.:
731 Reconstruction of climate and vegetation changes of Lake Bayanchagan (Inner
732 Mongolia): Holocene variability of the East Asian monsoon. Quaternary Research, 65,
733 411-420, 2006.

734 Jiang, W., Leroy, S. G., Ogle, N., Chu, G., Wang, L., and Liu, J.: Natural and authropogenic
735 forest fires recorded in the Holocene pollen record from a Jinchuan peat bog, northeastern
736 China, Palaeogeography, Palaeoclimatology, Palaeoecology, 261, 47-57, 2008.

737 Joussaume, S., and Taylor, K. E.: Status of the Paleoclimate Modeling Intercomparison
738 Project, Proceedings of the First International AMIP Scientific Conference, 425-430,
739 1995.

740 Joussaume, S., Taylor, K. E., Braconnot, P., Mitchell, J. F. B., Kutzbach, J. E., Harrison, S.
741 P., Prentice, I. C., Broccoli, A. J., Abe-Ouchi, A., Bartlein, P. J., Bonfils, C., Dong, B.,
742 Guiot, J., Herterich, K., Hewitt, C. D., Jolly, D., Kim, J. W., Kislov, A., Kitoh, A.,
743 Loutre, M. F., Masson, V., McAvaney, B., McFarlane, N., de Noblet, N., Peltier, W. R.,
744 Peterschmitt, J. Y., Pollard, D., Rind, D., Royer, J. F., Schlesinger, M. E., Syktus, J.,

745 Thompson, S., Valdes, P., Vettoretti, G., Webb, R. S., Wyputta, U.: Monsoon changes for
746 6000 years ago: Results of 18 simulations from the Paleoclimate Modeling
747 Intercomparison Project (PMIP), Geophysical Research Letters, 26, 856-862, 1999.

748 Kaplan, J. O., Bigelow, N. H., Bartlein, P. J., Christensen, T. R., Cramer, W., Harrison, S. P.,
749 Matveyeva, N. V., McGuire, A. D., Murray, D. F., Prentice, I. C., Razzhivin, V. Y.,
750 Smith, B., Anderson, P. M., Andreev, A. A., Brubaker, L. B., Edwards, M. E., and
751 Lozhkin, A. V.: Climate change and Arctic ecosystems: 2. Modeling, palaeodata-model
752 comparisons, and future projections, Journal of Geophysical Research: Atmospheres, 108,
753 8171, doi:10.1029/2002JD002559, 2003.

754 Kohfeld, K. E. and Harrison, S.: How well we can simulate past climates? Evaluating the
755 models using global palaeoenvironmental datasets, Quaternary Science Reviews, 19, 321-
756 346, 2000.

757 Kong, Z., Xu, Q., Yang, X., Sun, L., Liang, W.: Analysis of sporopollen assemblages of
758 Holocene alluvial deposits in the Yinmahe River Basin, Hebei Province, and preliminary
759 study on temporal and spatial changes of vegetation, Acta Phytoecologica Sinica, 24, 724,
760 2000 (in Chinese with English abstract).

761 Lee, Y., and Liew, M.: Pollen stratigraphy, vegetation and environment of the last glacial and
762 Holocene-A record from Toushe Basin, central Taiwan,
763 Palaeogeography, Palaeoclimatology, Palaeoecology, 287, 58-66, 2010.

764 Li, B., and Sun, J.: Vegetation and climate environment during Holocene in Xi'an region of
765 Loess Plateau, China, Marine Geology and Quaternary Geology, 3, 125-132, 2005 (in
766 Chinese with English abstract).

767 Li, C., Wu, Y., and Hou, X.: Holocene vegetation and climate in Northeast China revealed
768 from Jingbo Lake sediment, Quaternary International, 229, 67-73, 2011.

769 Li, L., Lin, P., Yu, Y., Wang, B., Zhou, T., Liu, L., Liu, J., Bao, Q., Xu, S., Huang, W., Xia,
770 K., Pu, Y., Dong, L., Shen, S., Liu, Y., Hu, N., Liu, M., Sun, W., Shi, X., Zheng, W., Wu,
771 B., Song, M., Liu, H., Zhang, X., Wu, G., Xue, W., Huang, X., Yang, G., Song, Z., and
772 Qiao, F.: The flexible global ocean-atmosphere-land system model, Grid-point Version 2:
773 FGOALS-g2, Advances in Atmospheric Sciences, 30, 543-560, 2013.

774 Li, Q., Wu, H., Guo, Z., Yu, Y., Ge, J., Wu, J., Zhao, D., and Sun, A.: Distribution and
775 vegetation reconstruction of the deserts of northern China during the mid-Holocene,
776 Geophysical Research Letter, 41, 2184-5191, 2014.

777 Li, X., and Liu, J.: Holocene vegetational and environmental changes at Mt. Luoji, Sichuan,
778 Acta Geographica Sinica, 1, 44-51, 1988 (in Chinese with English abstract).

779 Li, X., Zhao, K., Dodson, J., and Zhou, X.: Moisture dynamics in central Asia for the last
780 15 kyr: new evidence from Yili Valley, Xinjiang, NW China, Quaternary Science
781 Reviews, 30, 23-34, 2011.

782 Li, X., Zhou, J., and Dodson, J.: The vegetation characteristics of the ‘yuan’ area at Yaoxian
783 on the loess plateau in china over the last 12 000 years. Review of Palaeobotany &
784 Palynology, 124, 1-7, 2003.

785 Li, X., Zhou, W., An, Z., and Dodson, J.: The vegetation and monsoon variations at the
786 desert-loess transition belt at Midiwan in northern China for the last 13 ka, Holocene, 13,
787 779-784, 2003.

788 Li, Z., Hai, Y., Zhou, Y., Luo, R., Zhang, Q.: Pollen Component of Lacustrain Deposit and its
789 Palaeo-environment Significance in the Downstream Region of Urumqi Riever since
790 30Ka BP, Arid Land Geography, 24, 201-205, 2001 (in Chinese with English abstract).

Liu, H., Cui, H., Tian, Y., and Xu, L.: Temporal-spatial variances of Holocene precipitation at the Marginal area of the East Monsoon influences from pollen evidence, Acta Botanica Sinica, 44, 864-871, 2002 (in Chinese with English abstract).

Liu, H., Tang, X., Sun, D., and Wang, K.: Palynofloras of the Dajiuhu Basin in Shennongjia mountains during the last 12.5 ka, Acta Micropalaeontologica Sinica, 1, 101-109, 2001 (in Chinese with English abstract).

Liu, J., Zhao, S., Cheng, J., Bao, J., and Yin, G.: A study of vegetation and climate evolution since the Holocene near the banks of the Qiangtang River in Hangzhou Bay, Earth Science Frontiers, 5, 235-245, 2007 (in Chinese with English abstract).

Liu, M., Huang, Y., and Kuo, M.: Pollen stratigraphy, vegetation and environment of the last glacial and Holocene-A record from Toushe Basin, central Taiwan, Quaternary International, 14, 16-33, 2006.

Liu, Y., Liu, J., and Han, J.: Pollen record and climate changing since 12.0ka B. P. in Erlongwan Maar Lake, Jilin province, Journal of Jilin University (Earth Science Edition), 39, 93-98, 2009 (in Chinese with English abstract).

Liu, Y., Zhang, S., Liu, J., You, H., and Han, J.: Vegetation and environment history of erlongwan Maar lake during the late Pleistocene on pollen record, Acta Micropalaeontologica Sinica, 25, 274-280, 2008 (in Chinese with English abstract).

Liu, Z., Harrison, S. P., Kutzbach, J. E., and Otto-Bliesner, B.: Global monsoons in the mid-Holocene and oceanic feedback, Climate Dynamics, 22, 157-182, 2004.

Liu, Z., Wang, Y., Gallimore, R., Gasse, F., Johnson, T., deMenocal, P., Adkins, J., Notaro, M., Prentice, I.C., Kutzbach, J., Jacob, R., Behling, P., Wang, L., and Ong, E.: Simulating

the transient evolution and abrupt change of Northern Africa atmosphere–ocean–terrestrial ecosystem in the Holocene, Quaternary Science Reviews, 26, 1818-1837, 2007.

Liu, Z., Zhu, J., Rosenthal, Y., Zhang, X., Otto-Bliesner, B. L., Timmermann, A., Smith, R. S., Lohmann, G., Zheng, W., and Elison Timm, O.: The Holocene temperature conundrum, Proceedings of the National Academy of Sciences, 111, E3501-E3505, 2014.

Lu, H., Wu, N., Liu, K.-b., Zhu, L., Yang, X., Yao, T., Wang, L., Li, Q., Liu, X., Shen, C., Li, X., Tong, G., and Jiang, H.: Modern pollen distributions in Qinghai-Tibetan Plateau and the development of transfer functions for reconstructing Holocene environmental changes, Quaternary Science Reviews, 30, 947-966, 2012.

Luo, H.: Characteristics of the Holocene sporopollen flora and climate change in the Coqên area, Tibet, Chengdu University of Technology, Master Dissertation, 2008 (in Chinese with English abstract).

Mann, M. E., Zhang, Z., Hughes, M. K., Bradley, R. S., Miller, S. K., Rutherford, S., and Ni, F.: Proxy-based reconstructions of hemispheric and global surface temperature variations over the past two millennia, Proceedings of the National Academy of Sciences, 105, 13252-13256, 2008.

Marchant, R., Cleef, A., Harrison, S. P., Hooghiemstra, H., Markgraf, V., Van Boxel, J., Ager, T., Almeida, L., Anderson, R., Baied, C., Behling, H., Berrio, J. C., Burbridge, R., Bjorck, S., Byrne, R., Bush, M., Duivenvoorden, J., Flenley, J., De Oliveira, P., Van Gee, B., Graf, K., Gosling, W. D., Harbele, S., Van Der Hammen, T., Hansen, B., Horn, S., Kuhry, P., Ledru, M. P., Mayle, F., Leyden, B., Lozano-Garcia, S., Melief, A. M., Moreno, P., Moar, N. T., Prieto, A., Van Reenen, G., Salgado-Labouriau, M., Schabitz, F., Schreve-Brinkman, E. J., and Wille, M.: Pollen-based biome reconstructions for Latin

America at 0, 6000 and 18 000 radiocarbon years ago, Climate of the Past, 5, 725-767, 2009.

Marcott, S., Shakun, J., U Clark, P., and Mix, A.: A Reconstruction of Regional and Global Temperature for the Past 11,300 Years, Science, 1198-1201, 2013.

Marsicek, J., Shuman, B.N., Bartlein, P.J., Shafer, S.L., and Brewer, S.: Reconciling divergent trends and millennial variations in Holocene temperatures, Nature, 554, 92-96, 2018.

Mauri, A., Davis, B. A. S., Collins, P. M., and Kaplan, J. O.: The climate of Europe during the Holocene: a gridded pollen-based reconstruction and its multi-proxy evaluation, Quaternary Science Reviews, 112, 109-127, 2015.

Ma, Y., Zhang, H., Pachur, H., Wunnemann, B., Li, J., and Feng, Z.: Late Glacial and Holocene vegetation history and paleoclimate of the Tengger Desert, northwestern China, Chinese Science Bulletin, 48, 1457-1463, 2003.

Members of the China Quaternary Pollen Data Base.: Pollen-based Biome reconstruction at Middle Holocene (6 ka BP) and Last Glacial Maximum (18 ka BP) in China, Acta Botanica Sinica, 42, 1201-1209, 2000 (in Chinese with English abstract).

MARGO Project Members: Constraints on the magnitude and patterns of ocean cooling at the Last Glacial Maximum, Nature Geoscience, 2, 127-130, 2009.

Meng, X., Zhu, D., Shao, Z., Han, J., Yu, J., Meng, Q., Lv, R., and Luo, P.: Paleoclimatic and Plaeoenvironmental Evolution Since Holocene in the Ningwu Area, Shanxi Province, Acta Geologica Sinica, 3, 316-323, 2007 (in Chinese with English abstract).

857 Ni, J., Sykes, M. T., Prentice, I. C., and Cramer, W.: Modelling the vegetation of China using
858 the process-based equilibrium terrestrial biosphere model BIOME3, Global Ecology and
859 Biogeography, 9, 463-479, 2000.

860 Ni, J., Yu, G., Harrison, S.P., Prentice, I. C.: Palaeovegetation in China during the late
861 Quaternary: Biome reconstructions based on a global scheme of plant functional types,
862 Palaeogeography, Palaeoclimatology, Palaeoecology, 289, 44-61, 2010.

863 Oguntunde, P. G., Ajayi, A. E., and Giesen, N.: Tillage and surface moisture effects on bare-
864 soil albedo of a tropical loamy sand, Soil and Tillage Research, 85, 107-114, 2006.

865 O'ishi, R., A. Abe‐Ouchi, I. C. Prentice, and S. Sitch.: Vegetation dynamics and plant CO_2
866 responses as positive feedbacks in a greenhouse world, Geophysical Research Letters, 36,
867 L11706, doi: 10.1029/2009GL038217, 2009.

868 Otto, J., T. Raddatz, M. Claussen, V. Brovkin, and V. Gayler.: Separation of atmosphere-
869 ocean-vegetation feedbacks and synergies for mid-Holocene climate, Geophysical
870 Research Letters, 36, L09701, doi: 10.1029/2009GL037482, 2009.

871 Peyron, O., Guiot, J., Cheddadi, R., Tarasov, P., Reille, M., De Beaulieu, J.L., Bottema, S.,
872 and Andrieu, Valerie. : Climatic reconstruction in Europe for 18,000 YR B.P. from pollen
873 data, Quaternary Research, 49, 183-196, 1998.

874 Peyron, O., Jolly, D., Bonnefille, R., Vincens, A., and Guiot, J.: Climate of East Africa 6000
875 ^{14}C yr B.P. as Inferred from Pollen Data, Quaternary Research, 54, 90-101, 2000.

876 Pickett Elizabeth, J., Harrison Sandy, P., Hope, G., Harle, K., Dodson John, R., Peter
877 Kershaw, A., Colin Prentice, I., Backhouse, J., Colhoun Eric, A., D'Costa, D., Flenley, J.,
878 Grindrod, J., Haberle, S., Hassell, C., Kenyon, C., Macphail, M., Martin, H., Martin
879 Anthony, H., McKenzie, M., Newsome Jane, C., Penny, D., Powell, J., Ian Raine, J.,

880 Southern, W., Stevenson, J., Sutra, J. P., Thomas, I., Kaars, S., and Ward, J.: Pollen-based
881 reconstructions of biome distributions for Australia, Southeast Asia and the Pacific
882 (SEAPAC region) at 0, 6000 and 18,000 ^{14}C yr BP, Journal of Biogeography, 31, 1381-
883 1444, 2004.

884 Prentice, I. C., Guiot, J., Huntley, B., Jolly, D., and Cheddadi, R.: Reconstructing biomes
885 from palaeoecological data: A general method and its application to European pollen data
886 at 0 and 6 ka, Climate Dynamics, 12, 185-194, 1996.

887 Prentice, I. C., and Jolly, D.: Mid-Holocene and glacial-maximum vegetation geography of
888 the northern continents and Africa, Journal of Biogeography, 27, 507-519, 2000.

889 Reimer, P. J., Bard, E., Bayliss, A., Beck, J. W., Blackwell, P. G., Ramsey, C. B., Buck, C. E.,
890 Cheng, H., Edwards, R. L., Friedrich, M., Grootes, P. M., Guilderson, T. P., Haflidason,
891 H., Hajdas, I., Hatté, C., Heaton, T. J., Hoffmann, D. L., Hogg, A. G., Hughen, K. A.,
892 Kaiser, K. F., Kromer, B., Manning, S. W., Niu, M., Reimer, R. W., Richards, D. A.,
893 Scott, E. M., Southon, J. R., Staff, R. A., Turney, C. S. M. and van der Plicht, J.: IntCal13
894 and Marine13 Radiocarbon Age Calibration Curves 0–50,000 Years cal BP, Radiocarbon,
895 55(4), 1869–1887, doi:DOI: 10.2458/azu_js_rc.55.16947, 2013.

896 Schmidt, G.A., Annan, J.D., Bartlein, P.J., Cook, B.I., Guilyardi, E., Hargreaves, J.C.,
897 Harrison, S.P., Kageyama, M., Legrande, A.N., Konecky, B.L., Lovejoy, S., Mann, M.E.,
898 Masson-Delmotte, V., Risi, C., Thompson, D., Timmermann, A., and Yiou, P.: Using
899 palaeo-climate comparisons to constrain future projections in CMIP5, Climate of the Past,
900 10, 221-250, 2014a.

901 Schmidt, G.A., Kelley, M., Nazarenko, L., Ruedy, R., Russell, G.L., Aleinov, I., Bauer, M.,
902 Bauer, S.E., Bhat, M.K., Bleck, R., Canuto, V., Chen, Y., Cheng, Y., Clune, T.L., Del
903 Genio, A., de Fainchtein, R., Faluvegi, G., Hansen, J.E., Healy, R.J., Kiang, N.Y., Koch,

D., Lacis, A.A., Legrande, A.N., Lerner, J., Lo, K.K., Matthews, E.E., Menon, S., Miller, R.L., Oinas, V., Oloso, A.O., Perlwitz, J.P., Puma, M.J., Putman, W.M., Rind, D., Romanou, A., Sato, M., Shindell, D.T., Sun, S., Syed Rahman, A., Tausnev, N., Tsigaridis, K., Under, N., Voulgarakis, A., Yao, M., and Zhang, J.: Configuration and assessment of the GISS ModelE2 contributions to the CMIP5 archive, Journal of Advances in Modeling Earth Systems, 6, 141-184, 2014b.

Shakun, J. D., Clark, P. U., He, F., Marcott, S. A., Mix, A. C., Liu, Z., Otto-Bliesner, B., Schmittner, A., and Bard, E.: Global warming preceded by increasing carbon dioxide concentrations during the last deglaciation, Nature, 484, 49-55, 2012.

Shen, C., Liu, K., Tang, L., Overpeck, J. T.: Quantitative relationships between modern pollen rain and climate in the Tibetan Plateau, Review of Palaeobotany and Palynology, 140, 61-77, 2006.

Shen, J., Jones, R. T., Yang, X., Dearing, J. A., and Wang, S.: The Holocene vegetation history of lake Erhai, Yunnan province southwestern china: the role of climate and human forcings, The Holocene, 16, 265-276, 2006.

Shen, J., Liu, X., Matsumoto, R., Wang, S., Yang, X., Tang, L., and Shen, C.: Multi-index high-resolution paleoclimatic evolution of sediments in Qinghai Lake since the late glacial period, Science in China Series D: Earth Sciences, 6, 582-589, 2004 (in Chinese with English abstract).

Shu, J., Wang, W., and Chen, Y.: Holocene vegetation and environment changes in the NW Taihu Plain, Jiangsu Province, East China, Acta Micropalaeontologica Sinica, 2, 210-221, 2007 (in Chinese with English abstract).

926 Shu, Q., Xiao, J., Zhang, M., Zhao, Z., Chen, Y., and Li, J.: Climate Change in Northern
927 Jiangsu Basin since the Last Interglacial: Geological Science and Technology
928 Information, 5, 59-64, 2008 (in Chinese with English abstract).

929 Song, M., Zhou, C., and Ouyang, H.: Simulated distribution of vegetation types in response to
930 climate change on the Tibetan Plateau, Journal of Vegetation Science, 16, 341-350, 2005.

931 Sun, A., and Feng, Z.: Holocene climate reconstructions from the fossil pollen record at Qigai
932 Nuur in the southern Mongolian Plateau, The Holocene, 23, 1391-1402, 2013.

933 Sun, L., Xu, Q., Yang, X., Liang, W., Sun, Z., and Chen, S.: Vegetation and environmental
934 changes in the Xuanhua Basin of Hebei Province since Postglacial, Journal of
935 Geomechanics, 4, 303-308, 2001 (in Chinese with English abstract).

936 Sun, Q., Zhou, J., Shen, J., Cheng, P., Wu, F., and Xie, X.: Mid-Holocene environmental
937 characteristics recorded in the sediments of the Bohai Sea in the northern environmental
938 sensitive zone, Science in China Series D: Earth Sciences, 9, 838-849, 2006 (in Chinese
939 with English abstract).

940 Sun, X., and Xia, Z.: Paleoenvironment Changes Since Mid-Holocene Revealed by a
941 Palynological Sequence from Sihenan Profile in Luoyang, Henan Province, Acta
942 Scientiarum Naturalium Universitatis Pekinensis, 2, 289-294, 2005 (in Chinese with
943 English abstract).

944 Sun. X., Wang. F., and Sun. C.: Pollen-climate response surfaces of selected taxa from
945 Northern China, Science in China Series D: Earth Sciences, 39, 486, 1996.

946 Swann, A. L., Fung, I. Y., Levis, S., Bonan, G. B., and Doney, S. C.: Changes in Arctic
947 vegetation amplify high-latitude warming through the greenhouse effect, Proceedings of
948 the National Academy of Sciences, 107, 1295-1300, 2010.

949 Sykes, M.T., Prentice, I.C., and Laarif, F.: Quantifying the impact of global climate change on
950 potential natural vegetation, Climatic Change, 41, 37–52, 1999.

951 Tang, L., and An, C.: Holocene vegetation change and pollen record of drought events in the
952 Loess Plateau, Progress in Natural Science, 10,1371-1382, 2007 (in Chinese with English
953 abstract).

954 Tang, L., and Shen, C.: Holocene pollen records of the Qinghai-Xizang Plateau, Acta
955 Micropalaeontologica Sinica, 4, 407-422, 1996 (in Chinese with English abstract).

956 Tang, L., Shen, C., Kong, Z., Wang, F., and Liao, K.: Pollen evidence of climate during the
957 last glacial maximum in Eastern Tibetan Plateau, Journal of Glaciology, 2, 37-44, 1998
958 (in Chinese with English abstract).

959 Tang, L., Shen, C., Li, C., Peng, J., and Liu, H.: Pollen-inferred vegetation and environmental
960 changes in the central Tibetan Plateau since 8200 yr B.P., Science in China Series D:
961 Earth Sciences, 5, 615-625, 2009 (in Chinese with English abstract).

962 Tao, S., An, C., Chen, F., Tang, L., Wang, Z., Lv, Y., Li, Z., Zheng, T., and Zhao, J.:
963 Vegetation and environment since the 16.7cal ka B.P. in Balikun Lake, Xinjiang, China,
964 Chinese Science Bulletin, 11, 1026-1035, 2010 (in Chinese with English abstract).

965 Taylor, K.E., Crucifix, M., Braconnot, P., Hewitt, C. D., Doutriaux. C., Broccoli, A. J.,
966 Mitchell, J. F. B., Webb, M. J.: Estimating shortwave radiative forcing and response in
967 climate models, Journal of Climate, 20, 2530-2543, 2007.

968 Taylor, K.E., Stouffer, R.J., Meehl, G.A.: An overview of CMIP5 and the experiment design,
969 Bulletin of the American Meteorological Society, 93, 485-498, 2012.

970 Voldoire, A., Sanchez-Gomez, E., Salas y Melia, D., Decharme, B., Cassou, C.,Senesi, S.,
971 Valcke, S., Beau, I., Alias, A., Chevallier, M., Deque, M., Deshayes, J., Douville, H.,

Fernandez, E., Madec, G., Maisonnave, E., Moine, M., Planton, S., Saint-Martin, D., Szopa, S., Tyteca, S., Alkama, R., Belamari, S., Braun, A., Coquart, L., and Chauvin, F.: The CNRM-CM5.1 global climate model: description and basic evaluation, Climate Dynamics, 40, 2091-2121, 2012.

Wang, H., Liu, H., Zhu, J., and Yin, Y.: Holocene environmental changes as recorded by mineral magnetism of sediments from Anguli-nuur Lake, southeastern Inner Mongolia Plateau, China, Palaeogeography, Palaeoclimatology, Palaeoecology, 285, 30-49, 2010.

Wang, S., Lv, H., and Liu, J.: Environmental characteristics of the early Holocene suitable period revealed by the high-resolution sporopollen record of Huguangyan Lake, Chinese Science Bulletin, 11, 1285-1291, 2007 (in Chinese with English abstract).

Wang, X., Wang, J., Cao, L., Yang, J., Yang, X., Peng, Z., and Jin, G.: Late Quaternary Pollen Records and Climate Significance in Guangzhou, Acta Scientiarum Naturalium Universitatis Sunyatseni, 3, 113-121, 2010 (in Chinese with English abstract).

Wang, X., Zhang, G., Li, W., Zhang, X., Zhang, E., and Xiao, X.: Environmental changes during early-middle Holocene from the sediment record of the Chaohu Lake, Anhui Province, Chinese Science Bulletin, 53, 153-160, 2008.

Wang, Y., Wang, S., Jiang, F., and Tong, G.: Palynological records in Xipu section, Yangyuan, Journal of Geomechanics, 2, 171-175, 2003 (in Chinese with English abstract).

Wang, Y., Wang, S., Zhao, Z., Qin, Y., Ma, Y., Sun, J., Sun, H., and Tian, M.: Vegetation and Environmental Changes in Hexiqten Qi of Inner Mongolia in the Past 16000 Years, Acta Geoscientica Sinica, 5, 449-453, 2005 (in Chinese with English abstract).

Wang, Y., Zhao, Z., Qiao, Y., Wang, S., Li, C., and Song, L.: Paleoclimatic and paleoenvironmental evolution since the late glacial epoch as recorded by sporopollen from

995 the Hongyuan peat section on the Zoigê Plateau, northern Sichuan, China, Geological
996 Bulletin of China, 7, 827-832, 2006 (in Chinese with English abstract).

997 Watanabe, S., Hajima, T., Sudo, K., Nagashima, T., Takemura, T., Okajima, H., Nozawa, T.,
998 Kawase, H., Abe, M., Yokohata, T., Ise, T., Sato, H., Kato, E., Takata, K., Emori, S., and
999 Kawamiya, M.: MIROC-ESM 2010: model description and basic results of CMIP5-
1000 20c3m experiments, Geoscientific Model Development, 4, 845-872, 2011.

1001 Webb, III. T.: Global paleoclimatic data base for 6000 yr BP, Brown Univ., Providence, RI
1002 (USA). Dept. of Geological Sciences, DOE/EV/10097-6; Other: ON: DE85006628 United
1003 States Other: ON: DE85006628 NTIS, PC A08/MF A01. HEDB English, 1985.

1004 Wen, R., Xiao, J., Chang, Z., Zhai, D., Xu, Q., Li, Y. and Itoh, S.: Holocene precipitation and
1005 temperature variations in the East Asian monsoonal margin from pollen data from Hulun
1006 Lake in northeastern Inner Mongolia, China, Boreas, 39, 262-272, 2010.

1007 Weninger, B., Jöris, O., Danzeglocke, U.: CalPal-2007, Cologne Radiocarbon Calibration and
1008 Palaeoclimate Research Package, http://www.calpal.de/, 2007.

1009 Wischnewski, J., Mischke, S., Wang, Y., and Herzschuh, U.: Reconstructing climate
1010 variability on the northeastern Tibetan Plateau since the last Lateglacial – a multi-proxy,
1011 dual-site approach comparing terrestrial and aquatic signals, Quaternary Science Reviews,
1012 30, 82-97, 2011.

1013 Wohlfahrt, J., Harrison, S. P., and Braconnot, P.: Synergistic feedbacks between ocean and
1014 vegetation on mid- and high-latitude climates during the mid-Holocene, Climate
1015 Dynamics, 22, 223-238, 2004.

1016 Wu, H., Guiot, J., Brewer, S., and Guo, Z.: Climatic changes in Eurasia and Africa at the last
1017 glacial maximum and mid-Holocene: reconstruction from pollen data using inverse
1018 vegetation modeling, Climate Dynamics, 29, 211-229, 2007.

1019 Wu, H., Luo, Y., Jiang, W., Li, Q., Sun, A., and Guo, Z.: Paleoclimate reconstruction from
1020 pollen data using inverse vegetation approach: Validation of model using modern data,
1021 Quaternary Sciences, 36, 520-529, 2016 (in Chinese with English abstract).

1022 Wu, H., Ma, Y., Feng, Z., Sun, A., Zhang, C., Li, F., and Kuang, J.: A high resolution record
1023 of vegetation and environmental variation through the last ~25,000 years in the western
1024 part of the Chinese Loess Plateau, Palaeogeography, Palaeoclimatology, Palaeoecology,
1025 273, 191-199, 2009.

1026 Xia, Y.: Preliminary study on vegetational development and climatic changes in the Sanjiang
1027 Plain in the last 12000 years, Scientia Geographica Sinica, 8, 241-249, 1988 (in Chinese
1028 with English abstract).

1029 Xia, Z., Chen, G., Zheng, G., Chen, F., and Han, J.: Climate background of the evolution from
1030 Paleolithic to Neolithic cultural transition during the last deglaciation in the middle
1031 reaches of the Yellow River, Chinese Science Bulletin, 47, 71-75, 2002.

1032 Xiao, J., Lv, H., Zhou, W., Zhao, Z., and Hao, R.: Pollen Vegetation and Environmental
1033 Evolution of the Great Lakes in Jiangxi Province since the Last Glacial Maximum,
1034 Science in China Series D: Earth Sciences, 6, 789-797, 2007 (in Chinese with English
1035 abstract).

1036 Xiao, J., Xu, Q., Nakamura, T., Yang, X., Liang, W., and Inouchi, Y.: Holocene vegetation
1037 variation in the Daihai Lake region of north-central China: a direct indication of the Asian
1038 monsoon climatic history, Quaternary Science Reviews, 23, 1669-1679, 2004.

1039 Xiao, X., Haberle, S. G., Shen, J., Yang, X., Han, Y., Zhang, E., and Wang, S.: Latest
1040 Pleistocene and Holocene vegetation and climate history inferred from an alpine
1041 lacustrine record, northwestern Yunnan Province, southwestern China, Quaternary
1042 Science reviews, 86, 35-48, 2014.

1043 Xie, Y., Li, C., Wang, Q., and Yin, H.: Climatic Change since 9 ka B. P.: Evidence from
1044 Jiangling Area, Jianghan Plain, China, Scientia Geographica Sinica, 2, 199-204, 2006 (in
1045 Chinese with English abstract).

1046 Xin, X., Wu, T., and Zhang, J.: Introduction of CMIP5 experiments carried out with the
1047 climate system models of Beijing climate Center, Advances in Climate Change Research,
1048 4, 41-49, 2013.

1049 Xu, J.: Analysis of the Holocene Loess Pollen in Xifeng Area and its Vegetation Evolution,
1050 Capital Normal University, Master Dissertation, 2006 (in Chinese with English abstract).

1051 Xu, Q., Chen, S., Kong, Z., and Du, N.: Preliminary discussion of vegetation succession and
1052 climate change since the Holocene in the Baiyangdian Lake district, Acta Phytoecologica
1053 and Geobotanica Sinica, 2, 65-73, 1988 (in Chinese with English abstract).

1054 Xu, Q., Yang, Z., Cui, Z., Yang, X., and Liang.: A Study on Pollen Analysis of Qiguoshan
1055 Section and Ancestor Living Environment in Chifeng Area, Nei Mongol, Scientia
1056 Geographica Sinica, 4, 453-456, 2002 (in Chinese with English abstract).

1057 Xu, Y.: The assemblage of Holocene spore pollen and its environment in Bosten Lake area
1058 Xinjiang, Arid land Geography, 2, 43-49, 1998 (in Chinese with English abstract).

1059 Xue, S., and Li, X.: Holocene vegetation characteristics of the southern Loess Plateau in the
1060 Weihe River valley in China, Review of Palaeobotany & Palynology, 160 46-52, 2010.

1061 Yang, J., Cui, Z., Yi, Zhao., Zhang, W., and Liu, K.: Glacial Lacustrine Sediment's Response
1062 to Climate Change since Holocene in Diancang Mountain, Acta Geographica Sinica, 4,
1063 525-533, 2004 (in Chinese with English abstract).

1064 Yang, X., Wang, S., and Tong, G.: Character of anology and changes of monsoon climate
1065 over the last 10000 years in Gucheng Lake, Jiangsu province, Journal of Integrative Plant
1066 Biology, 7, 576-581, 1996 (in Chinese with English abstract).

1067 Yang, Y., and Wang, S.: Study on mire development and paleoenvironment change since
1068 8.0ka B.P. in the northern part of the Sangjiang Plain, Scientia Geographica Sinica, 23,
1069 32-38, 2003 (in Chinese with English abstract).

1070 Yang, Y., Huang, C., Wang, S., and Kong, Z: Study on the mire development and
1071 palaeogeographical environment change since the early period of the Holocene in the east
1072 part of the Xiliaohe Plain, Scientia Geographica Sinica, 21, 242-249, 2001 (in Chinese
1073 with English abstract).

1074 Yang, Z.: Reconstruction of climate and environment since the Holocene in Diaojiaohaizi
1075 Lake Area, Daqing Mountains,Inner Mongolia, Acta Ecologica Sinica, 4, 538-543, 2001
1076 (in Chinese with English abstract).

1077 Yu, L., Wang, N., Cheng, H., Long, H., and Zhao, Q.: Holocene environmental change in the
1078 marginal area of the Asian monsoon: a record from Zhuye Lake, NW china, Boreas, 38,
1079 349-361, 2009.

1080 Yukimoto, S., Adachi, Y., Hosaka, M., Sakami, T., Yoshimura, H., Hirabara, M., Tanaka,
1081 T.Y., Shindo, E., Tsujino, H., Deushi, M., Mizuta, R., Yabu, S., Obata, A., Nakano, H.,
1082 Koshiro, T., Ose, T., and Kitoh, A.: A new global climate model of the meteorological
1083 research institute: MRI-CGCM3-model description and basic performance, Journal of the
1084 Meterological Society of Japan, 90A, 23-64, 2012.

1085 Zhang, W., Mu, K., Cui, Z., Feng, J., and Yang, J.: Record of the environmental change since
1086 Holocene in the region of Gongwang mountain, Yunan Province, Earth and Environment,
1087 4, 343-350, 2007 (in Chinese with English abstract).

1088 Zhang, Y. G., Pagani, M., and Liu, Z.: A 12-Million-Year Temperature History of the tropical
1089 Pacific Ocean, Science, 344, 84-87, 2014.

1090 Zhang, Y., and Yu, S.: Palynological assemblages of late Quaternary from the Shenzhen
1091 region and its paleoenvironment evolution, Marine Geology & Quaternary Geology, 2,
1092 109-114, 1999 (in Chinese with English abstract).

1093 Zhang, Y., Jia, L., and Lyu, B.: Studies on Evolution of Vegetation and Climate since 7000
1094 Years ago in Estuary of Changjiang River Region, Marine Science Bulletin, 3, 27-34,
1095 2004 (in Chinese with English abstract).

1096 Zhang, Y., Song, M., and Welker, J. M.: Simulating Alpine Tundra Vegetation Dynamics in
1097 Response to Global Warming in China, Global Warming, Stuart Arthur Harris (Ed.),
1098 ISBN: 978-953-307-149-7, InTech, 11, 221-250, 2010.

1099 Zhang, Z., Xu, Q., Li, Y., Yang, X., Jin, Z., and Tang, J.: Environmental changes of the Yin
1100 ruins area based on pollen analysis, Quaternary Science, 27, 461-468, 2007 (in Chinese
1101 with English abstract).

1102 Zhao, J., Hou, Y., Du, J., and Chen, Y.: Holocene environmental changes in the Guanzhong
1103 Plain, Arid Land Geography, 1, 17-22, 2003 (in Chinese with English abstract).

1104 Zhao, Y., Yu, Z., Chen, F., Ito, E., and Zhao, C.: Holocene vegetation and climate history at
1105 Hurleg Lake in the Qaidam Basin, northwest China, Review of Palaeobotany and
1106 palynology, 145, 275-288, 2007.

Zheng, R., Xu, X., Zhu, J., Ji, F., Huang, Z., Li, J.: Division of late Quaternary strata and analysis of palaeoenvironment in Fuzhou Basin, Seismology and Geology, 4, 503-513, 2002 (in Chinese with English abstract).

Zheng, X., Zhang, H., Ming, Q., Chang, F., Meng, H., Zhang, W., Liu, M., Shen, C.: Vegetational and environmental changes since 15ka B.P. recorded by lake Lugu in the southwest monsoon domain region, Quaternary Sciences, 6, 1314-1326, 2014 (in Chinese with English abstract).

Zhou, J., Liu, D., Zhuang, Z., Wang, Z., and Liu, L.: The sediment layers and the records of the Paleoenvironment in the Chaoyanggang Lagoon,Rongcheng City of Shandong Province Since Holocene Transgression, Periodical of Ocean University of China, 38, 803-808, 2008 (in Chinese with English abstract).

Zhu, C., Ma, C., Zhang, W., Zheng, C., Tan, L., Lu, X., Liu, K., and Chen, H.: Pollenrecord from Dajiuhu Basin of Shennongjia and environmental changes since 15.753 ka B.P., Quaternary Sciences, 5, 814-826, 2006 (in Chinese with English abstract).

Zou, S., Cheng, G., Xiao, H., Xu, B., and Feng, Z.: Holocene natural rhythms of vegetation and present potential ecology in the western Chinese Loess Plateau, Quaternary International, 194, 55-67, 2009.

1129 **Table 1. Basic information of the pollen dataset used in this study**

Site	Lat	Lon	Alt	Webb 1-7	Source
Sujiawan	35.54	104.52	1700	2	original data (Zou et al., 2009)
Xiaogou	36.10	104.90	1750	2	original data (Wu et al., 2009)
Dadiwan	35.01	105.91	1400	1	original data (Zou et al., 2009)
Sanjiaocheng	39.01	103.34	1320	1	Chen et al., 2006
Chadianpo	36.10	114.40	65	2	Z. Zhang et al., 2007
Qindeli	48.08	133.25	60	2	Yang and Wang, 2003
Fuyuanchuangye	47.35	133.03	56	3	Xia, 1988
Jingbo Lake	43.83	128.50	350	2	C. Li et al., 2011
Hani Lake	42.22	126.52	900	1	Cui et al., 2006
Jinchuan	42.37	126.43	662	5	Jiang et al., 2008
Maar Lake	42.30	126.37	724	1	Liu et al., 2009
Maar Lake	42.30	126.37	724	1	Liu et al., 2008
Xie Lake SO4	37.38	122.52	0	1	Zhou et al., 2008
Nanhuiheming Core	31.05	121.58	7	2	Jia and Zhang, 2006
Toushe	23.82	120.88	650	1	Liu et al., 2006
Dongyuan Lake	22.17	120.83	415	2	Lee et al., 2010
Yonglong CY	31.78	120.44	5	3	Zhang et al., 2004
Hangzhou HZ3	30.30	120.33	6	4	J. Liu et al., 2007
Xinhua XH1	32.93	119.83	2	3	Shu et al., 2008
ZK01	31.77	119.80	6	2	Shu et al., 2007
Chifeng	43.97	119.37	503	2	Xu et al., 2002
SZK1	26.08	119.31	9	1	Zheng et al., 2002
Gucheng	31.28	118.90	6	4	Yang et al., 1996
Lulong	39.87	118.87	23	2	Kong et al., 2000
Hulun Lake	48.92	117.42	545	1	Wen et al., 2010
CH-1	31.56	117.39	5	2	Wang et al., 2008
Sanyi profile	43.62	117.38	1598	4	Wang et al., 2005
Xiaoniuchang	42.62	116.82	1411	1	Liu et al., 2002
Haoluku	42.87	116.76	1333	2	Liu et al., 2002
Liuzhouwan	42.71	116.68	1410	7	Liu et al., 2002
Poyang Lake 103B	28.87	116.25	16	4	Jiang and Piperno, 1999
Baiyangdian	38.92	115.84	8	2	Xu et al., 1988
Bayanchagan	42.08	115.35	1355	1	Jiang et al., 2006
Huangjiapu	40.57	115.15	614	7	Sun et al., 2001
Dingnan	24.68	115.00	250	2	Xiao et al., 2007
Guang1	36.02	114.53	56	1	Z. Zhang et al., 2007
Angulinao	41.33	114.35	1315	1	H. Wang et al., 2010
Yangyuanxipu	40.12	114.22	921	6	Wang et al., 2003

Shenzhen Sx07	22.75	113.78	2	2	Zhang and Yu, 1999
GZ-2	22.71	113.51	1	7	X. Wang et al., 2010
Daihai99a	40.55	112.66	1221	2	Xiao et al., 2004
Daihai	40.55	112.66	1221	2	Sun et al., 2006
Sihenan profile	34.80	112.40	251	1	Sun and Xia, 2005
Diaojiaohaizi	41.30	112.35	2015	1	Yang et al., 2001
Ganhaizi	39.00	112.30	1854	3	Meng et al., 2007
Jiangling profile	30.35	112.18	37	1	Xie et al., 2006
Helingeer	40.38	111.82	1162	3	X. Li et al., 2011
Shennongjia2	31.75	110.67	1700	1	Liu et al., 2001
Huguangyan Maar Lake	21.15	110.28	59	2	Wang et al., 2007
Yaoxian	35.93	110.17	1556	2	Li et al., 2003a
Jixian	36.00	110.06	1005	6	Xia et al., 2002
Shennongjia Dajiu Lake	31.49	110.00	1760	2	Zhu et al., 2006
Qigai nuur	39.50	109.85	1300	1	Sun and Feng, 2013
Beizhuangcun	34.35	109.53	519	1	Xue et al., 2010
Lantian	34.15	109.33	523	1	Li and Sun, 2005
Bahanniao	39.32	109.27	1278	1	Guo et al., 2007
Midiwan	37.65	108.62	1400	1	Li et al., 2003b
Jinbian	37.50	108.33	1688	2	Cheng, 2011
Xindian	34.38	107.80	608	1	Xue et al., 2010
Nanguanzhuang	34.43	107.75	702	1	Zhao et al., 2003
Xifeng	35.65	107.68	1400	3	Xu, 2006
Jiyuan	37.13	107.40	1765	3	X. Li et al., 2011
Jiacunyuan	34.27	106.97	1497	2	Gong, 2006
Dadiwan	35.01	105.91	1400	1	Zou et al., 2009
Maying	35.34	104.99	1800	1	Tang and An, 2007
Huiningxiaogou	36.10	104.90	1750	2	Wu et al., 2009
Sujiawan	35.54	104.52	1700	2	Zou et al., 2009
QTH02	39.07	103.61	1302	1	Yu et al., 2009
Laotanfang	26.10	103.20	3579	2	W. Zhang et al., 2007
Hongshui River2	38.17	102.76	1511	1	Ma et al., 2003,
Ruoergai	33.77	102.55	3480	1	Cai, 2008
Hongyuan	32.78	102.52	3500	2	Wang et al., 2006
Dahaizi	27.50	102.33	3660	1	Li et al., 1988
Shayema Lake	28.58	102.22	2453	1	Tang and Shen, 1996
Luanhaizi	37.59	101.35	3200	5	Herzschuh et al., 2006
Lugu Lake	27.68	100.80	2692	1	Zheng et al., 2014
Qinghai Lake	36.93	100.73	3200	2	Shen et al., 2004
Dalianhai	36.25	100.41	2850	3	Cheng et al., 2010
Erhai ES Core	25.78	100.19	1974	1	Shen et al., 2006
Xianmachi profile	25.97	99.87	3820	7	Yang et al., 2004
TCK1	26.63	99.72	3898	1	Xiao et al., 2014

Yidun Lake	30.30	99.55	4470	4	Shen et al., 2006
Kuhai lake	35.30	99.20	4150	1	Wischnewski et al., 2011
Koucha lake	34.00	97.20	4540	2	Herzschuh et al., 2009
Hurleg	37.28	96.90	2817	2	Zhao et al., 2007
Basu	30.72	96.67	4450	3	Tang et al., 1998
Tuolekule	43.34	94.21	1890	1	An et al., 2011
Balikun	43.62	92.77	1575	1	Tao et al., 2010
Cuona	31.47	91.51	4515	3	Tang et al., 2009
Dongdaohaizi2	44.64	87.58	402	1	Li et al., 2001
Bositeng Lake	41.96	87.21	1050	1	Xu, 1998
Cuoqin	31.00	85.00	4648	4	Luo, 2008
Yili	43.86	81.97	928	2	X. Li et al., 2011
Bangong Lake	33.75	78.67	4241	1	Huang et al., 1996
Shengli	47.53	133.87	52	2	CQPD, 2000
Qingdeli	48.05	133.17	52	1	CQPD, 2000
Changbaishan	42.22	126.00	500	2	CQPD, 2000
Liuhe	42.90	125.75	910	7	CQPD, 2000
Shuangyang	43.27	125.75	215	1	CQPD, 2000
Xiaonan	43.33	125.33	209	1	CQPD, 2000
Tailai	46.40	123.43	146	5	CQPD, 2000
Sheli	45.23	123.31	150	4	CQPD, 2000
Tongtu	45.23	123.30	150	7	CQPD, 2000
Yueyawan	37.98	120.71	5	1	CQPD, 2000
Beiwangxu	37.75	120.61	6	1	CQPD, 2000
East Tai Lake1	31.30	120.60	3	1	CQPD, 2000
Suzhou	31.30	120.60	2	7	CQPD, 2000
Sun-Moon Lake	23.51	120.54	726	2	CQPD, 2000
West Tai Lake	31.30	119.80	1	1	CQPD, 2000
Changzhou	31.43	119.41	5	1	CQPD, 2000
Dazeyin	39.50	119.17	50	7	CQPD, 2000
Hailaer	49.17	119.00	760	2	CQPD, 2000
Cangumiao	39.97	118.60	70	1	CQPD, 2000
Qianhuzhuang	40.00	118.58	80	6	CQPD, 2000
Reshuitang	43.75	117.65	1200	1	CQPD, 2000
Yangerzhuang	38.20	117.30	5	7	CQPD, 2000
Mengcun	38.00	117.06	7	5	CQPD, 2000
Hanjiang-CH2	23.48	116.80	5	2	CQPD, 2000
Hanjiang-SH6	23.42	116.68	3	7	CQPD, 2000
Hanjiang-SH5	23.45	116.67	8	2	CQPD, 2000
Hulun Lake	48.90	116.50	650	1	CQPD, 2000
Heitutang	40.38	113.74	1060	1	CQPD, 2000
Zhujiang delta PK16	22.73	113.72	15	7	CQPD, 2000
Angulitun	41.30	113.70	1400	7	CQPD, 2000

Bataigou	40.92	113.63	1357	1	CQPD, 2000
Dahewan	40.87	113.57	1298	2	CQPD, 2000
Yutubao	40.75	112.67	1254	7	CQPD, 2000
Zhujiang delta K5	22.78	112.63	12	1	CQPD, 2000
Da-7	40.52	112.62	1200	3	CQPD, 2000
Hahai-1	40.17	112.50	1200	5	CQPD, 2000
Wajianggou	40.50	112.50	1476	4	CQPD, 2000
Shuidong Core A1	21.75	111.07	-8	2	CQPD, 2000
Dajahu	31.50	110.33	1700	2	CQPD, 2000
Tianshuigou	34.87	109.73	360	7	CQPD, 2000
Mengjiawan	38.60	109.67	1190	7	CQPD, 2000
Fuping BK13	34.70	109.25	422	7	CQPD, 2000
Yaocun	34.70	109.22	405	2	CQPD, 2000
Jinbian	37.80	108.60	1400	4	CQPD, 2000
Dishaogou	37.83	108.45	1200	2	CQPD, 2000
Shuidonggou	38.20	106.57	1200	5	CQPD, 2000
Jiuzhoutai	35.90	104.80	2136	7	CQPD, 2000
Luojishan	27.50	102.40	3800	1	CQPD, 2000
RM-F	33.08	102.35	3400	2	CQPD, 2000
Hongyuan	33.25	101.57	3492	1	CQPD, 2000
Wasong	33.20	101.52	3490	1	CQPD, 2000
Guhu Core 28	27.67	100.83	2780	7	CQPD, 2000
Napahai Core 34	27.80	99.60	3260	2	CQPD, 2000
Lop Nur	40.50	90.25	780	7	CQPD, 2000
Chaiwobao1	43.55	87.78	1100	2	CQPD, 2000
Chaiwobao2	43.33	87.47	1114	1	CQPD, 2000
Manasi	45.97	84.83	257	2	CQPD, 2000
Wuqia	43.20	83.50	1000	7	CQPD, 2000
Madagou	37.00	80.70	1370	2	CQPD, 2000
Tongyu	44.83	123.10	148	5	CQPD, 2000
Nanjing	32.15	119.05	10	2	CQPD, 2000
Banpo	34.27	109.03	395	1	CQPD, 2000
QL-1	34.00	107.58	2200	7	CQPD, 2000
Dalainu	43.20	116.60	1290	7	CQPD, 2000
Qinghai	36.55	99.60	3196	2	CQPD, 2000

Table 2. Earth's orbital parameters and trace gases as recommended by the PMIP3 project

Simulation	Orbital parameters			Trace gases		
	Eccentricity	Obliquity(°)	Longitude of the perihelion(°)	CO_2(ppmv)	CH_4(ppbv)	N_2O(ppbv)
PI	0,016724	23,446	102,04	280	760	270
MH	0,018682	24,105	0,87	280	650	270

Table 3. PMIP3 model characteristics and references

Model Name	*Modelling centre*	*Type*	*Grid*	*Reference*
BCC-CSM-1-1	BCC-CMA (China)	AOVGCM	Atm: 128×64×L26; Ocean: 360×232×L40	Xin et al. (2013)
CCSM4	NCAR (USA)	AOGCM	Atm: 288 × 192×L26; Ocean: 320×384×L60	Gent et al. (2011)
CNRM-CM5	CNRM&CERFACS (France)	AOGCM	Atm: 256 × 128×L31; Ocean: 362×292×L42	Voldoire et al. (2012)
CSIRO-Mk3-6-0	QCCCE, Australia	AOGCM	Atm: 192 × 96×L18; Ocean: 192×192×L31	Jeffrey et al. (2013)
FGOALS-g2	LASG-IAP (China)	AOVGCM	Atm: 128 × 60×L26; Ocean: 360×180×L30	Li et al. (2013)
FGOALS-s2	LASG-IAP (China)	AOVGCM	Atm: 128 × 108×L26; Ocean: 360×180×L30	Bao et al. (2013)
GISS-E2-R	GISS (USA)	AOGCM	Atm: 144 × 90×L40; Ocean: 288×180×L32	Schmidt et al. (2014a,b)
HadGEM2-CC	Hadley Centre (UK)	AOVGCM	Atm: 192 × 145×L60; Ocean: 360×216×L40	Collins et al. (2011)
HadGEM2-ES	Hadley Centre (UK)	AOVGCM	Atm: 192 × 145×L38; Ocean: 360×216×L40	Collins et al. (2011)
IPSL-CM5A-LR	IPSL (France)	AOVGCM	Atm: 96 × 96×L39; Ocean: 182×149×L31	Dufresne et al. (2013)
MIROC-ESM	Utokyo&NIES (Japan)	AOVGCM	Atm: 128×64×L80; Ocean: 256×192×L44	Watanabe et al. (2011)
MPI-ESM-P	MPI (Germany)	AOGCM	Atm: 196×98×L47; Ocean: 256×220×L40	Giorgetta et al. (2013)
MRI-CGCM3	MRI (Japan)	AOGCM	Atm: 320 × 160×L48; Ocean: 364×368×L51	Yukimoto et al. (2012)

Table 4. Important values for each plant life form used in the ΔV statistical calculation as assigned to the megabiomes

Megabiomes	*Life form*		
	Trees	**Grass/grass**	**Bare ground**
Tropical forest	1		
Warm mixed forest	1		
Temperate forest	1		
Boreal forest	1		
Grassland and dry shrubland	0.25	0.75	
Savanna and dry woodland	0.5	0.5	
Desert		0.25	0.75
Tundra		0.75	0.25

Table 5. Attribute values and the weights for plant life forms used by the ΔV statistic

Life form	*Attribute*			
Trees	Evergreen	Needle-leaf	Tropical	Boreal
Tropical forest	1	0	1	0
Warm mixed forest	0.75	0.25	0	0
Temperate forest	0.5	0.5	0	0.5
Boreal forest	0.25	0.75	0	1
Grassland and dry shrubland	0.75	0.25	0.75	0
Savanna and dry woodland	0.25	0.75	0	0.5
weights	0.2	0.2	0.3	0.3
Grass/Shrub	Warm	Arctic/alpine		
Grassland and dry shrubland	1	0		
Savanna and dry woodland	0.75	0		
Desert	1	0		
Tundra	0	1		
weights	0.5	0.5		
Bare Ground	Arctic/alpine			
Desert	0			
Tundra	1			
weight	1			

Table 6. Regression coefficients between the reconstructed climates by inverse vegetation models and observed meteorogical values

Climate parameter	Slope	Intercept	R	ME	RMSE
MAT	0..82±0..02	0.92±0.18	0.89	0.16	3.25
MTCO	0.81±0.01	-1.79±0.18	0.95	-0.17	3.19
MTWA	0.75±0.03	4.57±0.60	0.75	-0.19	4.02
MAP	1.15±0.02	32.90±18.41	0.94	138.01	263.88
Pjan	1.01±0.02	0.32±0.47	0.94	0.52	8.89
Pjul	1.30±0.03	-21.67±4.52	0.89	16.45	52.9

The climatic parameters used for regression are the actual values (data source: China Climate Bureau, China Ground Meteorological Record Monthly Report, 1951-2001). MAT annual mean temperature, MTCO mean temperature of the coldest month, MTWA mean temperature of the warmest month, MAP annual precipitation, RMSE the root-mean-square error of the residuals, ME mean error of the residuals, Pjan: precipitation of January, Pjul: precipitation of July, R is the correlation coefficient, ± stand error

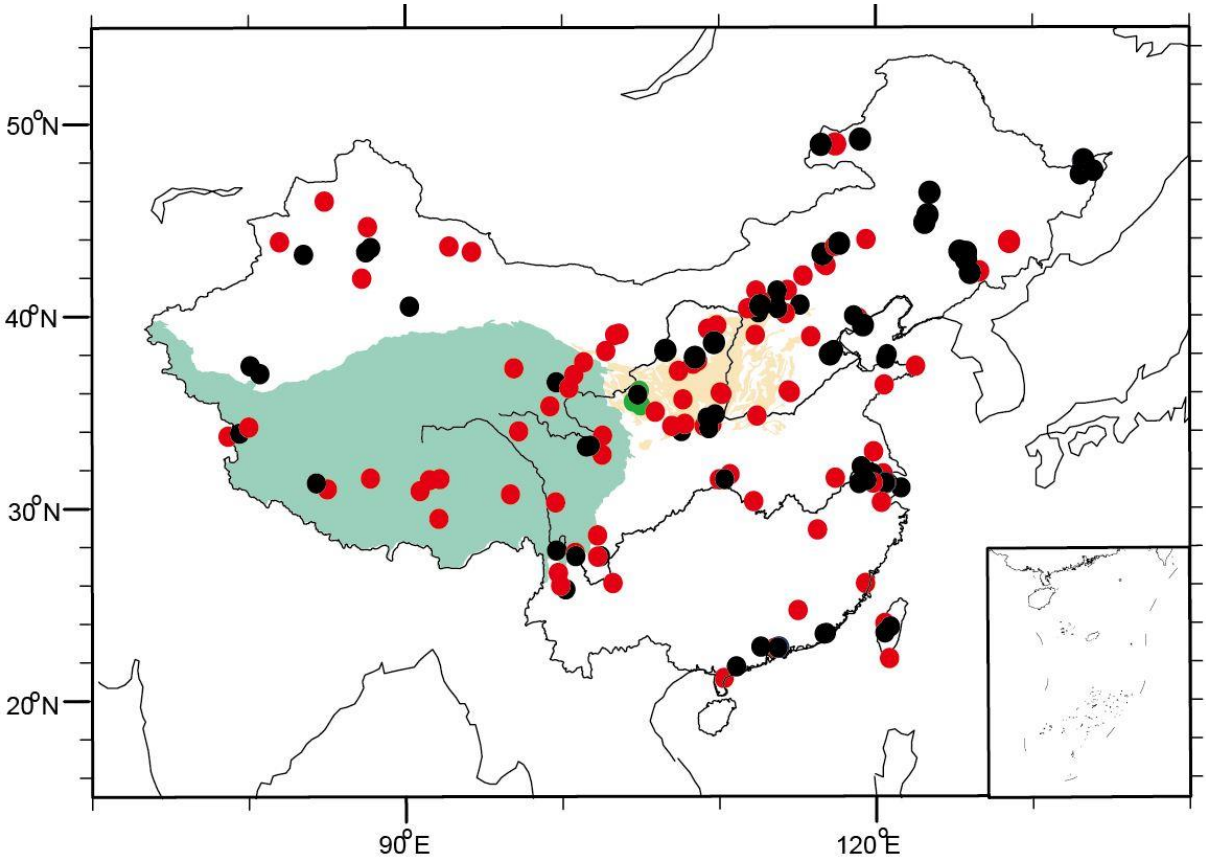

Figure 1. Distribution of pollen sites during mid-Holocene period in China. Black circle is the original China Quaternary Pollen Database, red circles are digitized ones from published papers, green circles represent the three original pollen data used in this study. The area with green color represents the Tibetan Plateau, yellow color for the Loess Plateau.

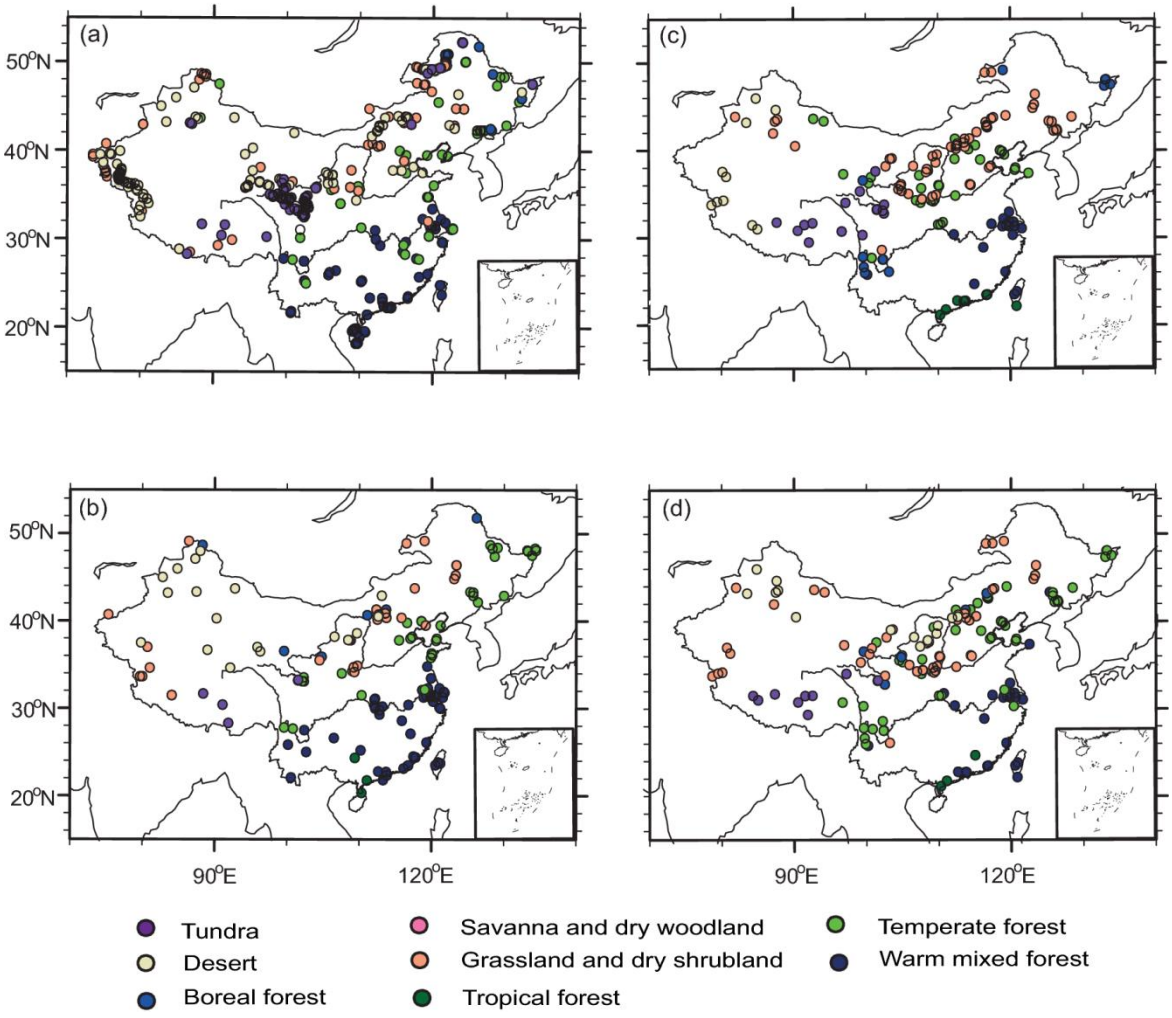

Figure 2. Comparison of megabiomes for PI (first row) and the MH (second row): (a,b) BIOME6000, (c,d) pollen data collected in this study.

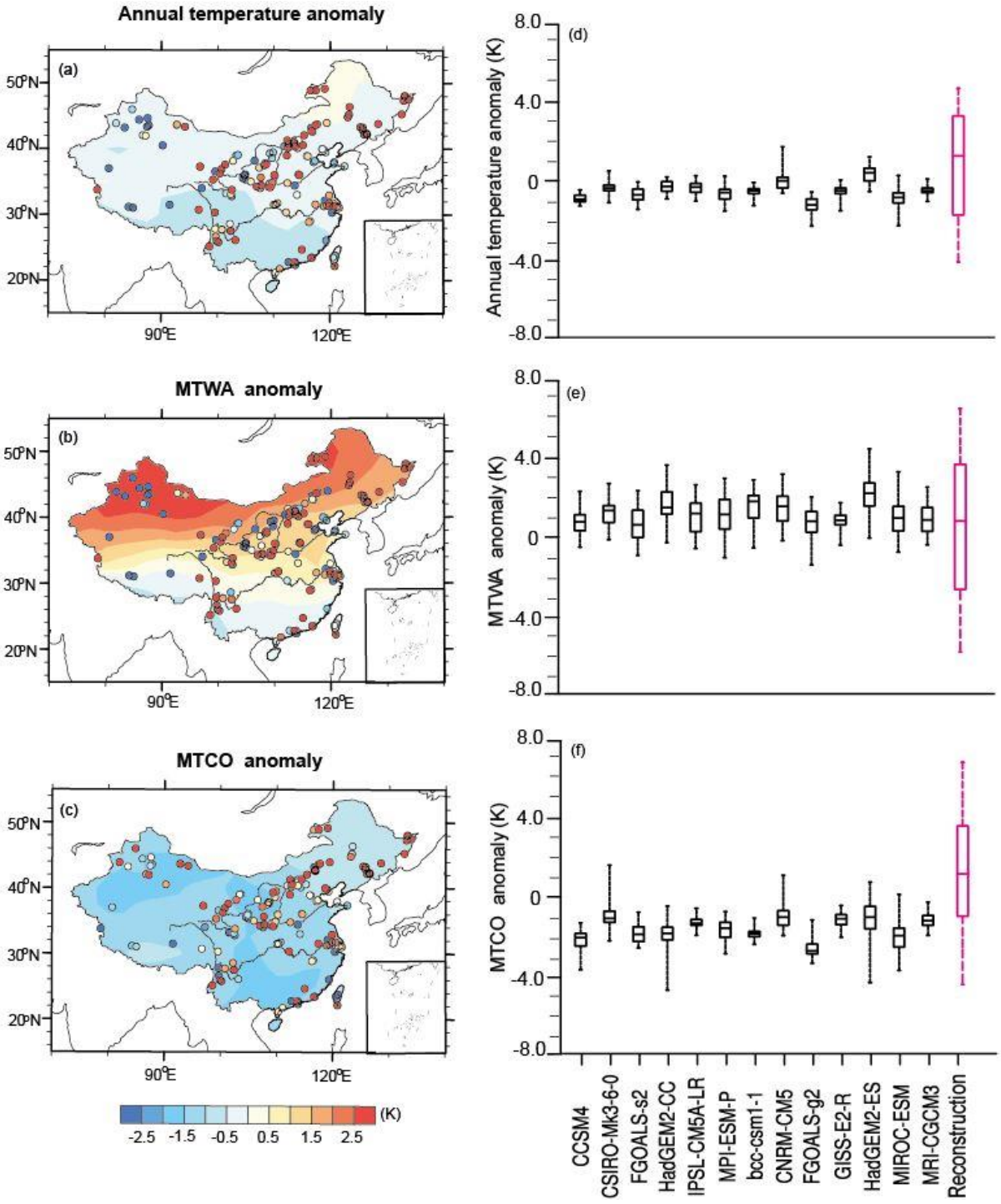

Figure 3. Model-data comparison for annual and seasonal (MTWA and MTCO) temperature (K). For the left panel (a-c), points represent the reconstruction from IVM, shades show the last 30-year means simulation results of multi-model ensemble (MME) for 13 PMIP3 models. The box-and-whisker plots (d-f) show the changes as shown by each PMIP3 model and the reconstruction. (d) considers changes in annual temperature, (e) indicates changes in MTWA, and (f) shows changes in MTCO. The lines in each box shows the median value from each set of measurements, the box shows the 25%-75% range, and the whiskers show the 90% interval (5th to 95th percentile).

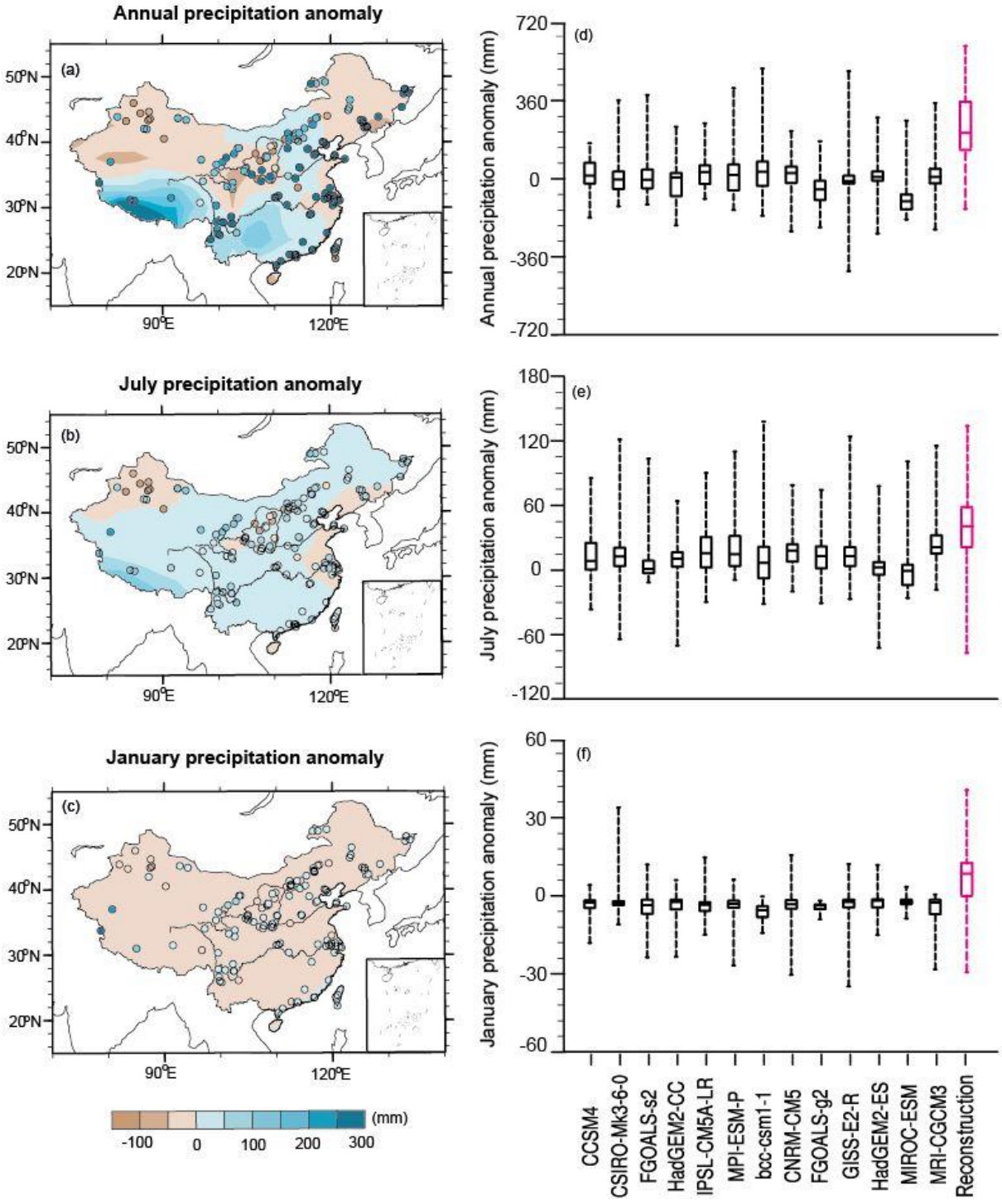

Figure 4. Model-data comparison for annual, July and January precipitation (mm). For the left panel (a,b), points represent the reconstruction from IVM, shades show the last 30-year means simulation results of multi-model ensemble (MME) for 13 PMIP3 models. The box-and-whisker plots (d-f) show the changes as shown by each PMIP3 model and the reconstruction. (d) considers changes in annual precipitation, (e) indicates changes in July precipitation, and (f) shows changes in January precipitation. The lines in each box shows the median value from each set of measurements, the box shows the 25%-75% range, and the whiskers show the 90% interval (5th to 95th percentile).

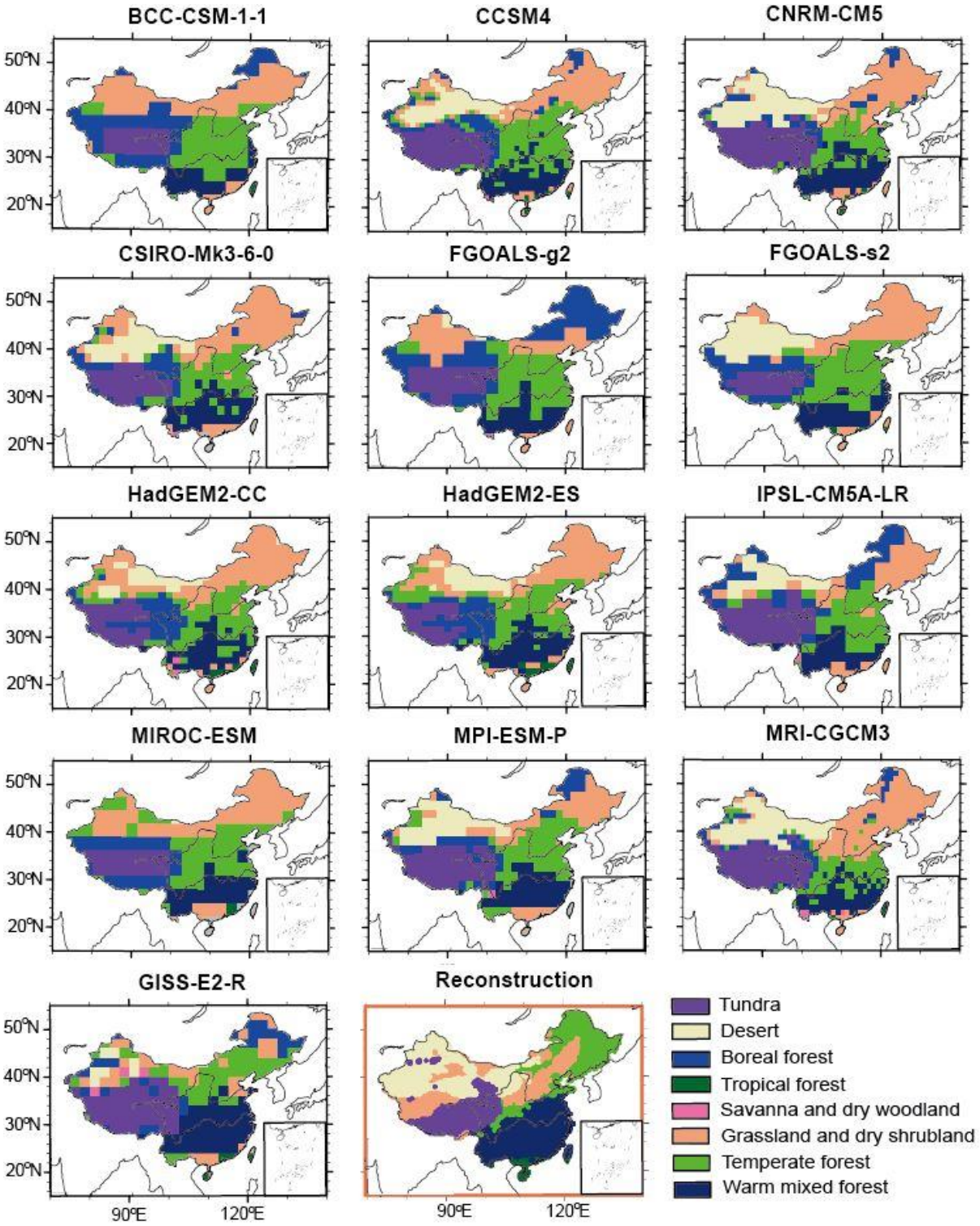

Figure 5. Comparison of interpolated megabiomes distribution (plot in red rectangle) with the simulated spatial pattern from BIOME4 for each model during mid-Holocene.

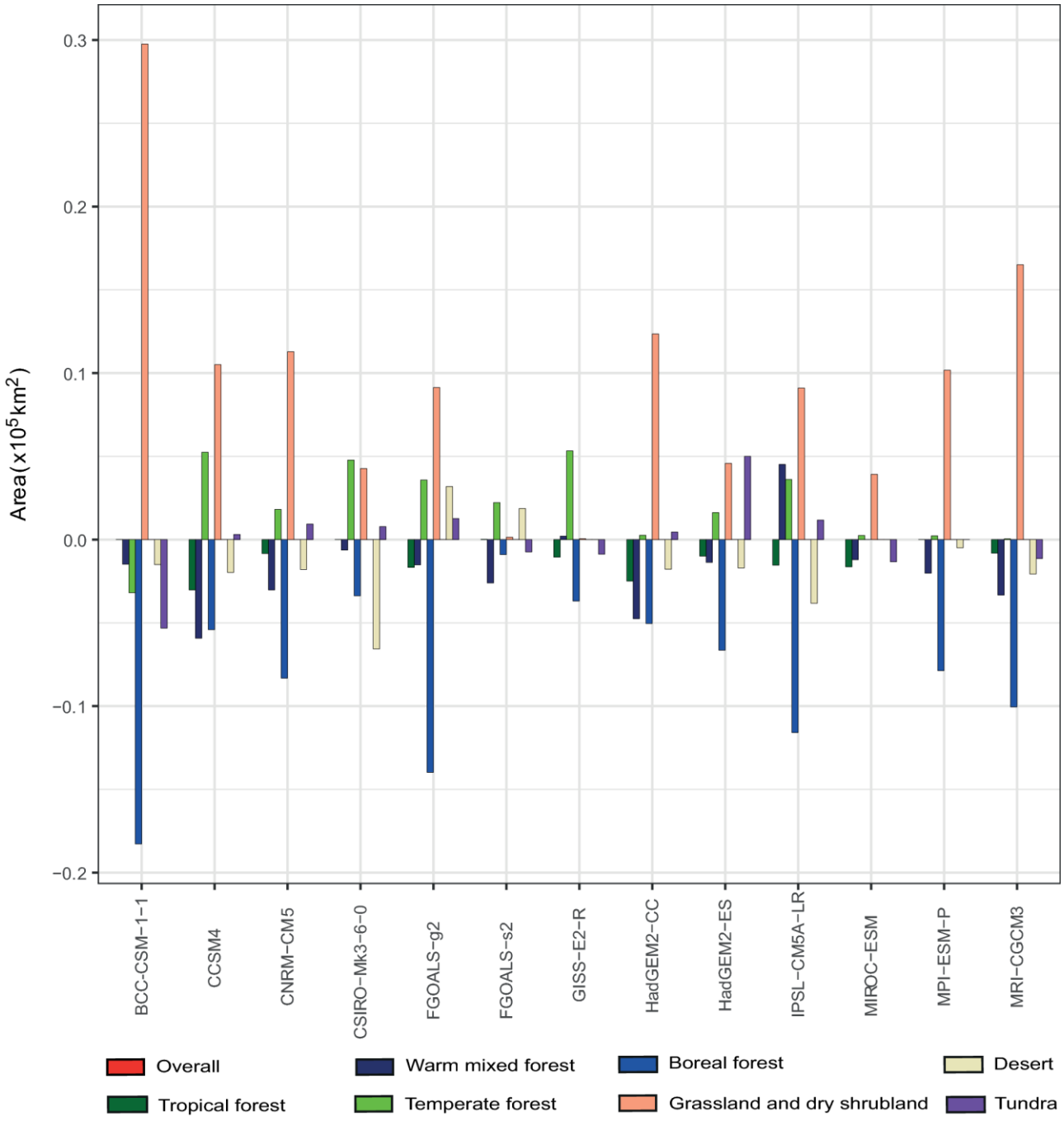

Figure 6. Changes in the extent of each megabiome as a consequence of simulated climate changes for each model, both expressed as change relative to the PI extent of same megabiome.

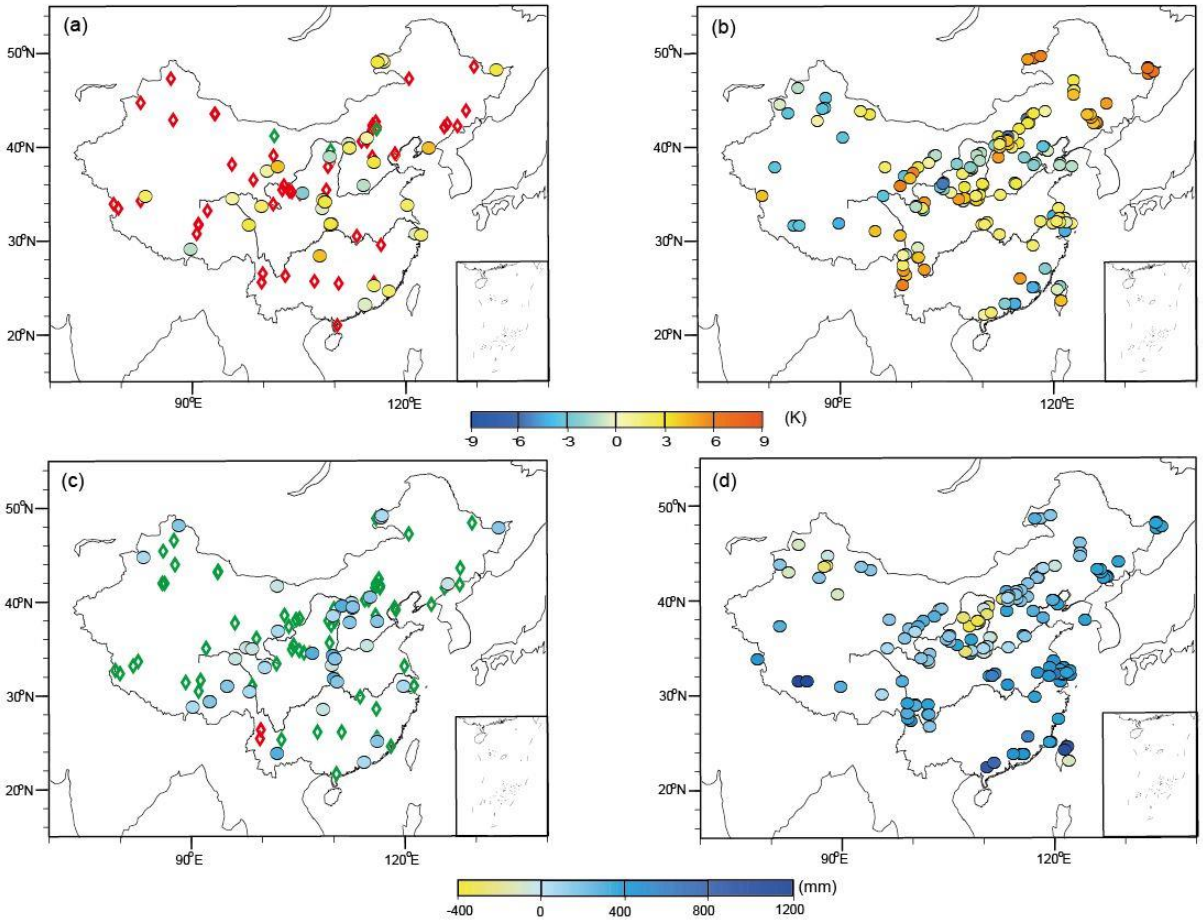

Figure 7. Comparison between the climate reconstruction and previous reconstruction over China. (a) Previous temperature results. Diamond is the qualitative reconstruction, red is the temperature increase and green is the temperature decrease; Circle is quantitative reconstruction; (b) Mean annual temperature reconstruction in this study; (c) Previous precipitation results, diamond is the qualitative reconstruction, red is the precipitation decrease and green is the precipitation increase; Circle is the quantitative reconstruction; (d) Mean annual precipitation reconstruction in this study.

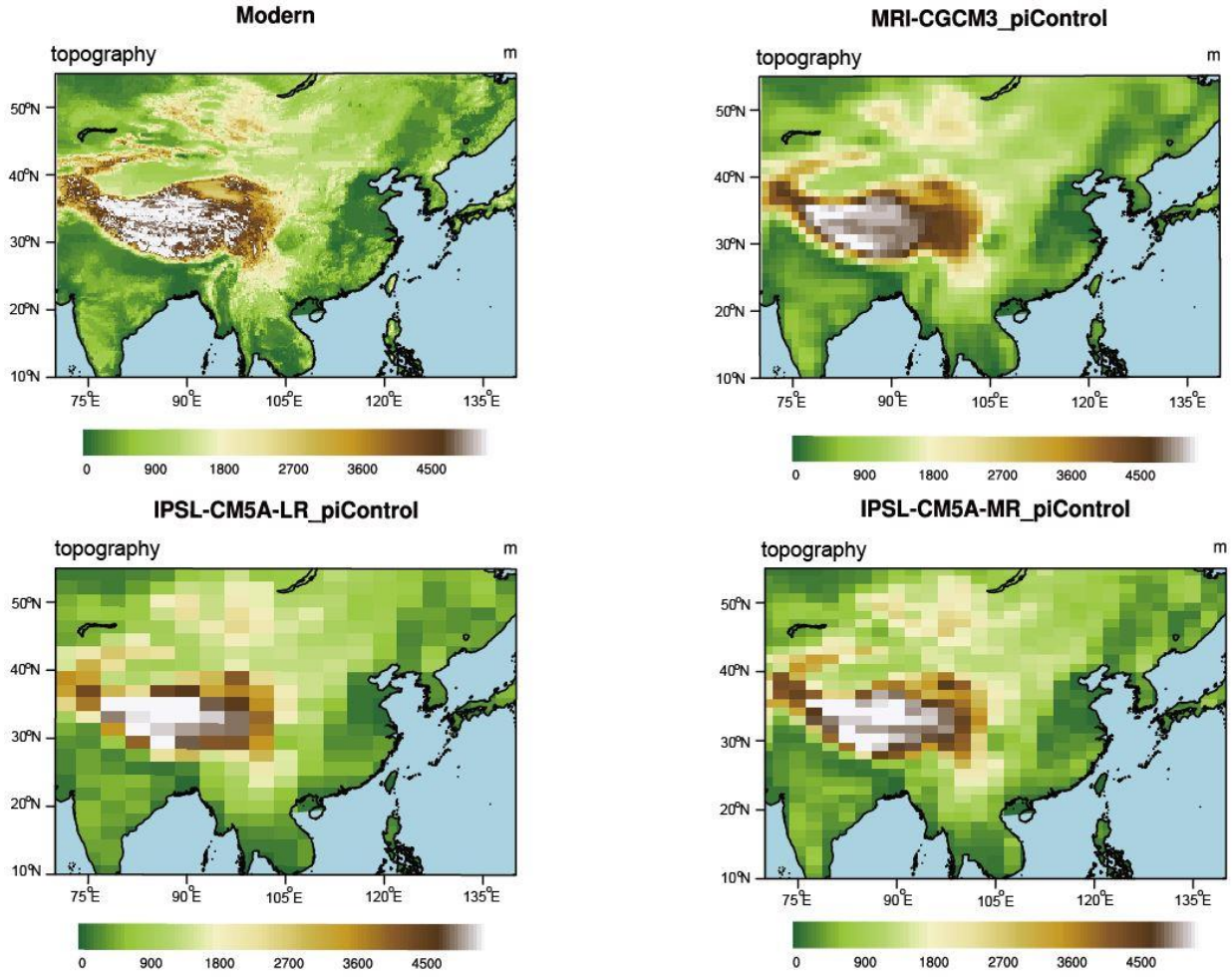

Figure 8. The topography comparison between models and observation.

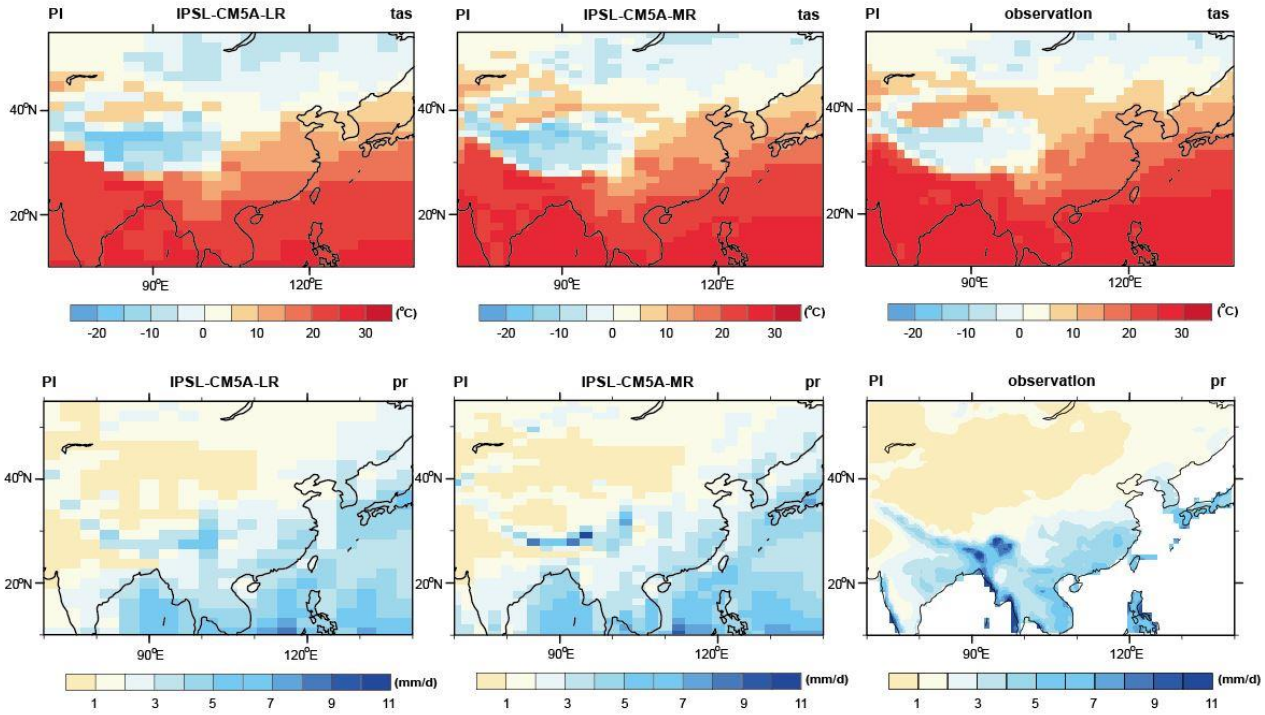

Figure 9. The preindustrial climate comparison between simulation and observation. Tas means temperature above 2m surface, pr means precipitation.

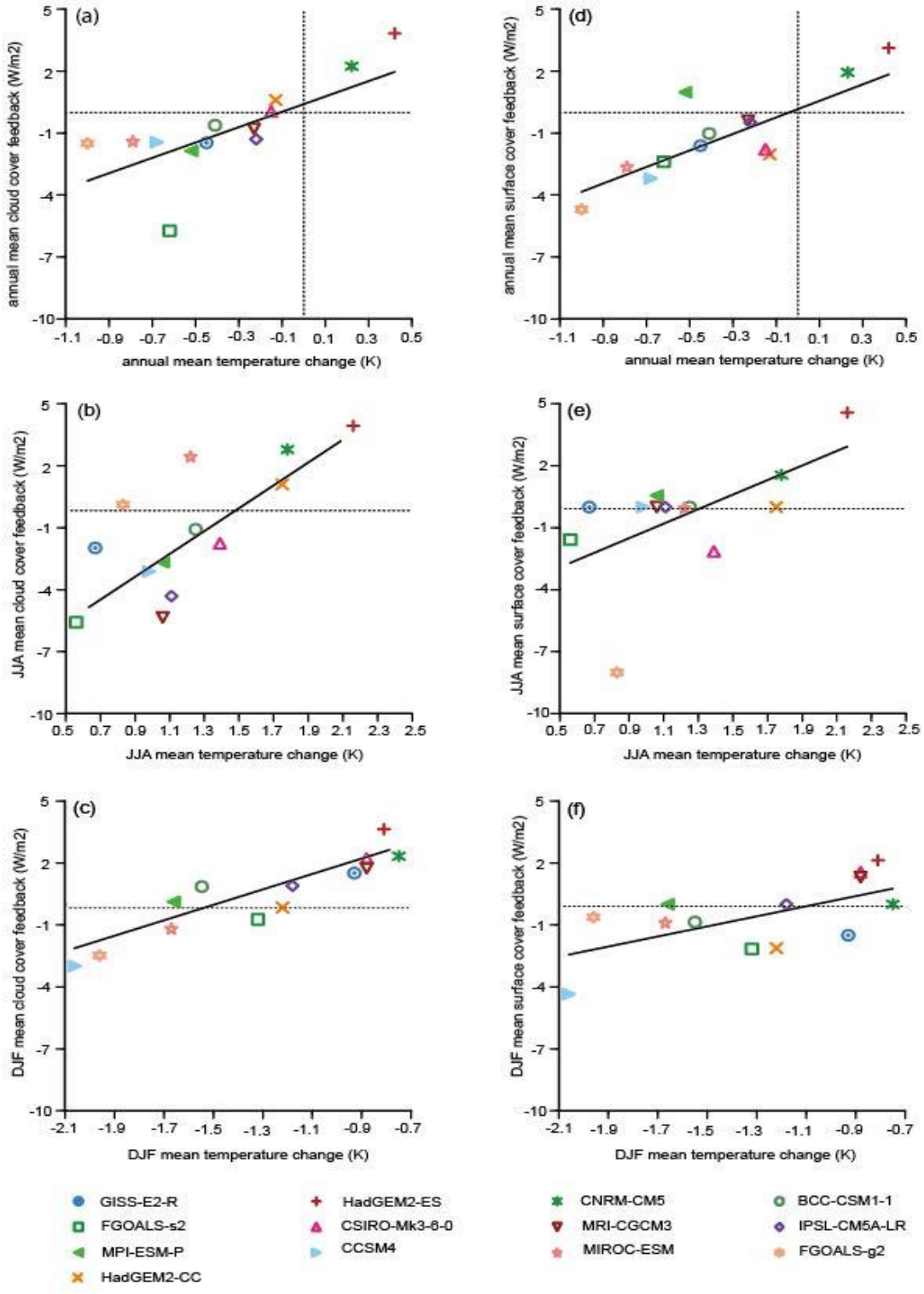

Figure 10. Scatter plots showing temperature, cloud cover feedback and surface albedo feedback changes during the MH. The values shown are the simulated 30-year mean anomaly (MH-PI) for the 13 models. **a**, annual mean temperature relative to the annual mean cloud cover feedback and d, annual surface albedo feedback. b, Summer (JJA) mean temperature relative to the summer mean cloud cover feedback and **e**, Summer surface albedo feedback. **c**, Winter (DJF) mean temperature relative to the summer mean cloud cover feedback and **f**, Winter surface albedo feedback. The horizontal and vertical lines in plots represent the value of 0.

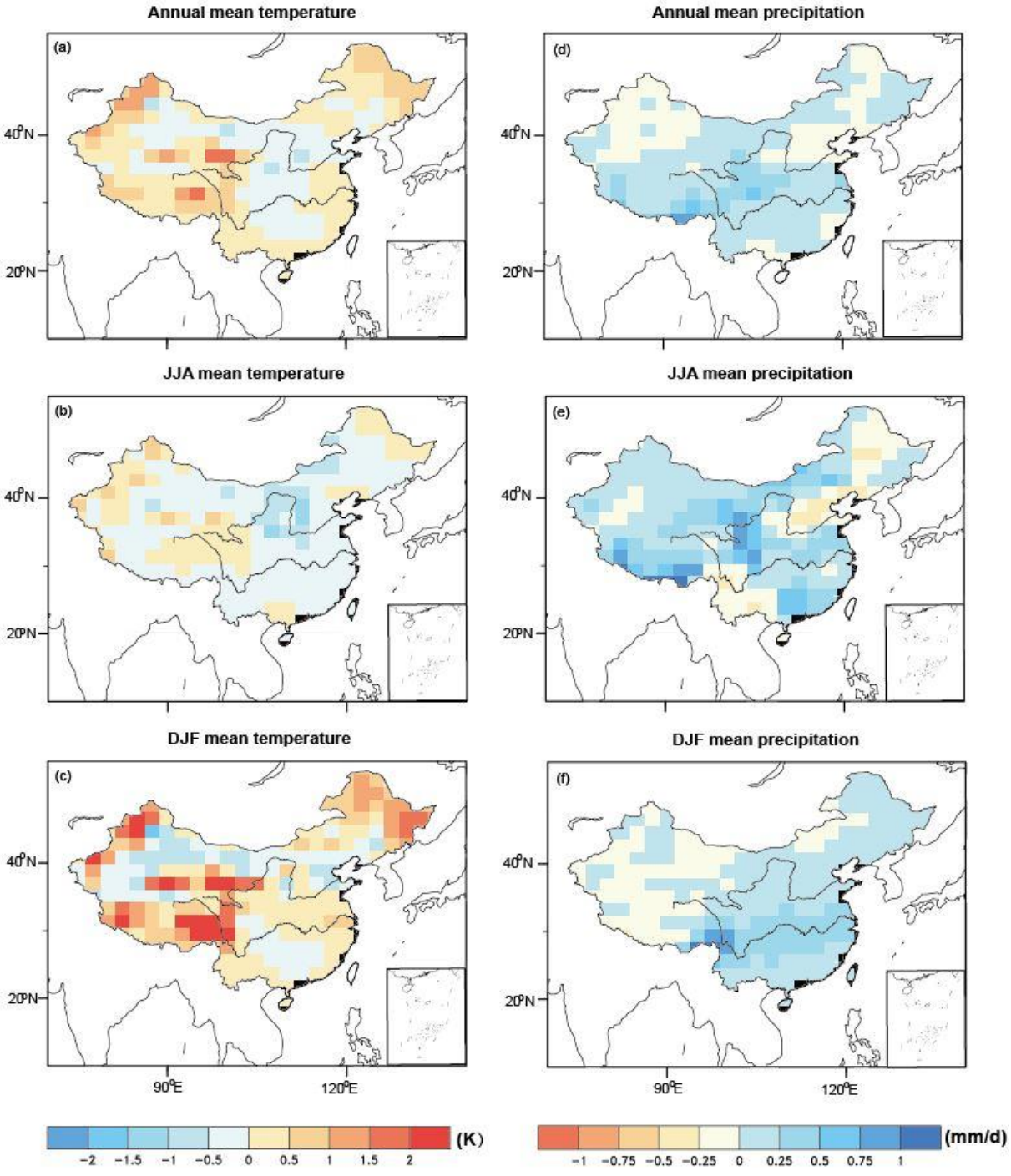

Figure 11. Climate anomalies between the two experiments (6 ka and 6 ka_VEG) conducted in CESM version 1.0.5. The anomalies (6 ka_VEG-6 ka) of temperature and precipitation at both annual and seasonal scale are presented, and all these climate variables are calculated as the last 50-year means from two simulations.